UNIVERSITY OF TARTU

Faculty of Science and Technology

Institute of Technology

Sergei Tolbin

Investigation of the Atomic Layer Deposition principles: Effects of growth parameters on SiO_2 thin films using hexakis(ethylamino)disilane (AHEAD) as a silicon precursor

Bachelor's Thesis (12 ECTS)

Curriculum Science & Technology

Supervisor(s):

Researcher, PhD Taivo Jõgiaas

Tartu 2025

Investigation of the Atomic Layer Deposition principles: Effects of growth parameters on SiO_2 thin films using hexakis(ethylamino)disilane (AHEAD) as a silicon precursor

This thesis investigates the deposition of silicon dioxide (SiO_2) thin films using Atomic Layer Deposition (ALD), with a focus on optimizing process parameters to improve film thickness, uniformity, and chemical composition.

Hexakis(ethylamino)disilane (AHEAD) was used as the silicon precursor, and ozone as the oxidant. The study systematically examines the effects of growth temperature, precursor evaporation temperature, and pulse durations on film properties, with characterization performed using ellipsometry and X-ray fluorescence (XRF).

This work contributes to a better understanding of the ALD process using the AHEAD precursor and provides practical guidance for tuning deposition parameters to fabricate high-quality SiO_2 films for semiconductor and nanotechnology applications.

Keywords: Atomic layer deposition, silicon dioxide, hexakis(ethylamino)disilane, thin films

CERCS: T150 Materials technology. P250 Condensed matter: structure, thermal and mechanical properties, crystallography, phase equilibria.

Aatomkihtsadestuse põhimõtete uurimine: kasvuprogrammi parameetrite mõju SiO_2 õhukestele kiledele, kasutades räniallikana heksakis(etüülamino)disilaani (AHEAD)

See lõputöö uurib ränidioksiidi (SiO_2) õhukeste kilede sadestamist aatomkihilise sadestamise (ALD) meetodil, keskendudes protsessiparameetrite optimeerimisele kile paksuse, ühtluse ja keemilise koostise parandamiseks.

Räniallikana kasutati heksakis(etüülamino)disilaani (AHEAD) ja oksüdeerijana osooni. Uurimus käsitleb süstemaatiliselt kasvutemperatuuri, eelkäaine aurustamistemperatuuri ja impulsside kestuse mõju kile omadustele, kusjuures iseloomustamine viidi läbi ellipsomeetria ja röntgenfluorestsentsi (XRF) abil.

See töö aitab paremini mõista ALD-protsessi AHEAD-eeskäaine kasutamisel ning pakub praktilisi juhiseid sadestamisparameetrite häälestamiseks kvaliteetsete SiO_2-kilede valmistamiseks pooljuhtide ja nanotehnoloogia rakenduste jaoks.

Võtmesõnad: Aatomkihtsadestamine, ränidioksiid, heksakis(etüülamino)disilaan, õhukesed kiled

CERCS: T150 Materials technology. P250 Condensed matter: structure, thermal and mechanical properties, crystallography, phase equilibria.

TABLE OF CONTENTS

ABBREVIATIONS AND NOTATIONS 6

1 Introduction 7

2 Literature review 8

2.1 ALD principles 8

2.1.1 Thermal ALD 9

2.2 Importance of ALD and its applications 10

2.3 Factors affecting thin film growth 12

2.3.1 Growth models 13

2.3.2 Precursor selection 14

2.3.3 ALD Window 16

2.3.4 Pulse length and ALD cycles 16

2.4 SiO_2 literature review 18

2.4.1 Deposition techniques and precursors 18

2.4.2 Silicon oxide deposition from hexakis(ethylamino)disilane 20

3 Characterization of silicon oxide films 21

3.1 Ellipsometry 22

3.2 XRF 24

4 Experiment set-up 27

5 Results and discussion 29

5.1 Deposition gradients and chemical compositions 29

5.1.1 Deposition gradients 30

5.1.2 Chemical composition 31

5.2 Temperature dependence 33

5.2.1 Growth temperature influence on film thickness 33

5.2.2 Precursor evaporation temperature 34

5.3 Precursor pulse length influence 35

5.3.1 Dose of AHEAD 35

5.3.2 Dose of ozone 35

5.4 Conclusion 36

6 SUMMARY 39

References 40

7 Appendix 44

7.1 Reactor description and set up 44

7.2 Variations of ALD techniques 50

7.2.1 Spatial ALD 50

7.2.2 Area selective ALD 51

7.2.3 Photo-assisted ALD 53

7.3 SiO_2 additions from literature review 54

7.3.1 SiO_2 in electronics 54

7.3.2 SiO_2 in optics 56

7.4 Anomalies 57

ABBREVIATIONS AND NOTATIONS

ALD – Atomic layer deposition

DRAM - Dynamic Random-Access Memory

MRAM - Magnetoresistive Random Access Memory

FeRAM - Ferroelectric Random-Access Memory

LCDs - Liquid crystal displays

OLEDs - Organic light-emitting diodes

AHEAD - Hexakis(ethylamino)disilane

RRAM - Resistive random-access memory

CVD – Chemical vapour deposition

PVD – Physical vapour deposition

TMA - Trimethylaluminum

T-ALD – Thermal ALD

PE-ALD – Enhanced plasma ALD

S-ALD – Spatial ALD

P-ALD – Photo assisted/Photochemical ALD

AS-ALD - Area-selective ALD

PE-ALD - Photochemical Etching ALD

MOSFETs - Metal-Oxide-Semiconductor Field-Effect Transistors

T(g) – temperature of growth

T(evap) – temperature of evaporation

1 Introduction

Atomic layer deposition (ALD) is recognized as a leading technique for producing precise thin films with diverse characteristics. Originating in the 1960s and 1970s, ALD continues to be a cornerstone in modern semiconductor fabrication, due to its exceptional versatility in controlling film thickness and uniformity, which are crucial for manufacturing advanced semiconductor devices and nanoscale electronic components [1-2]. ALD enables precise tuning of material properties through the selection of suitable precursor chemistries, adjusting deposition temperatures for precursor evaporation and growth processes, as well as the time under which the reaction takes place. This allows us to tailor film compositions and functionalities. The unique self-limiting reaction mechanism and possibility of ALD to deposit at significantly lower temperatures distinguishes it from other deposition methods like CVD and PVD, making ALD highly attractive for nanotechnology application and semiconductor device fabrication [3]. The thin film properties can be controlled in many ways, starting from choice of precursor with specific characteristics to defects that can occur during film growth. ALD offers control over these properties due to its precise deposition mechanism, allowing the creation of films with tailored characteristics such as thickness, composition, and structure. Moreover, ALD's capability to deposit materials atom by atom or molecule by molecule allows the fabrication of ultra-thin films with exceptional uniformity over large substrate areas. This uniformity is crucial for ensuring consistent device performance and reliability, especially in advanced semiconductor manufacturing processes where even minor variations can have significant consequences. ALD, as a versatile technique, is capable of depositing thin films of various materials, including metal oxides (Al_2O_3, HfO_2, etc.), metal nitrides (TiN, AlN, etc.), metal sulfides (CuS, ZnS, etc.), semiconductors (Si, Ge, etc.), dielectrics (SiO_2, Ta_2O_5), organic materials (polymers, organic-inorganic hybrids) and metals (Pt, Ag, etc.) [3].

Silicon dioxide (SiO_2) is widely used material in thin film applications because of its compatibility with semiconductor manufacturing processes. Specifically, SiO_2 thin films serve as the electrical insulation layer for gate structures in silicon-based integrated transistors, playing a vital role in modern electronic devices [4-5]. Advancements in deposition techniques, such as chemical vapor deposition (CVD) and atomic layer deposition (ALD), have further enhanced the uniformity, thickness control, and

scalability of SiO_2 thin films, enabling their integration into increasingly complex and miniaturized electronic circuits. As semiconductor technology continues to evolve, SiO_2 thin films are expected to continue to be a fundamental building block in the fabrication of high-performance integrated circuits and other electronic components. This research aims to investigate the principles of the ALD deposition technique and to learn how growth parameters affect thin-film depositions, using the example of SiO_2 films deposition using a silicon precursor hexakis(ethylamino)disilane (AHEAD) and ozone as the oxygen precursor.

2 Literature review

2.1 ALD principles

Atomic Layer Deposition (ALD) is a leading film deposition technique based on sequential self-terminating reactions at the gas-solid interface. It ensures layer-by-layer deposition with atomic precision, where a finite number of surface reaction sites determine the deposition of a finite number of surface species. Each precursor gas is introduced individually and reacts with the substrate surface to initiate nucleation and layer formation. During the ALD deposition cycle, there are alternating precursor introduction and purge steps, during which excess material and by-products are expelled from the chamber using an inert gas to ensure a clean substrate surface for the next precursor cycle (Figure 1)[6].

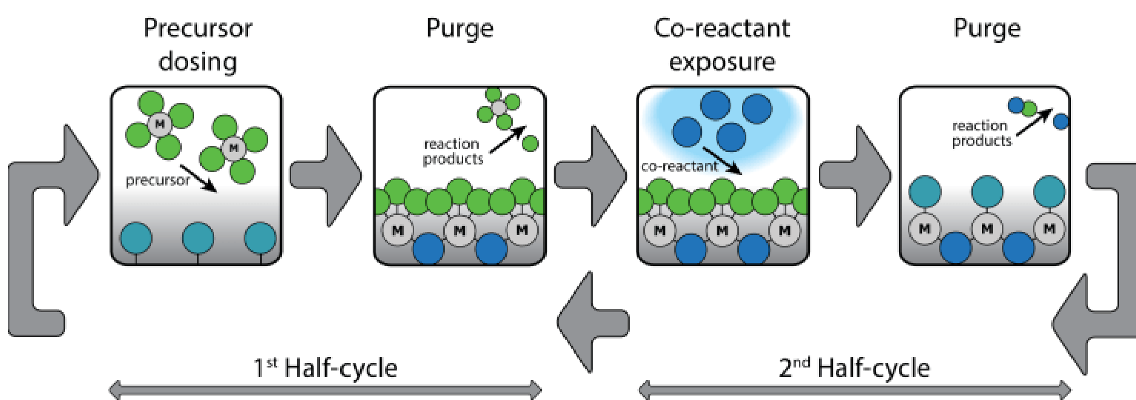

Figure 1. ALD Cycle example. (Adopted from [6])

This separation allows precise control over film thickness and composition, resulting in uniformity and accurate in film deposition. ALD is an indispensable tool in thin film fabrication for diverse applications [1-3, 7]. Additionally, the self-limiting nature of ALD reactions provides exceptional step coverage and conformal deposition, particularly on high-aspect ratio structures. Although different surface areas may react at various rates due to differing precursor gas fluxes, the self-limiting reactions ensure uniformity by adsorbing and desorbing from completed reaction sites before proceeding to unreacted areas. Consequently, ALD films exhibit remarkable smoothness and conformance to the substrate, with continuous, pinhole-free characteristics ideal for dielectric applications. Notably, ALD processes offer scalability to large substrates and enable the parallel processing of multiple substrates. The gaseous nature of ALD precursors ensures uniform coverage regardless of substrate geometry. However, the primary limitation of ALD lies in the size of the reaction chamber, as the process relies on surface reactions rather than gas-phase interactions. This sequential nature of surface reactions minimizes the risk of gas-phase precursors reactions leading to particle formation and subsequent granular film deposition, resulting the production of high-quality, homogeneous thin films [7].

2.1.1 Thermal ALD

While most reactions in ALD are derived from chemical vapor deposition (CVD) and can be summarise to reaction “A + B = product”, the implementation of ALD diverges significantly. In CVD, reactants flow directly into the deposition chamber, whereas ALD introduces its reactants separately. This distinct sequential deposition mechanism enables precise control over film thickness at the atomic scale, rendering thermal ALD particularly suitable for applications demanding ultra-thin films with uniform properties. One of the most extensively studied examples of thermal ALD is the deposition of Al_2O_3 thin films, frequently described in scientific literature [2, 7-11]. This film is deposited with the use of H2O and TMA (trimetylaluminum) (Figure 2) [8].

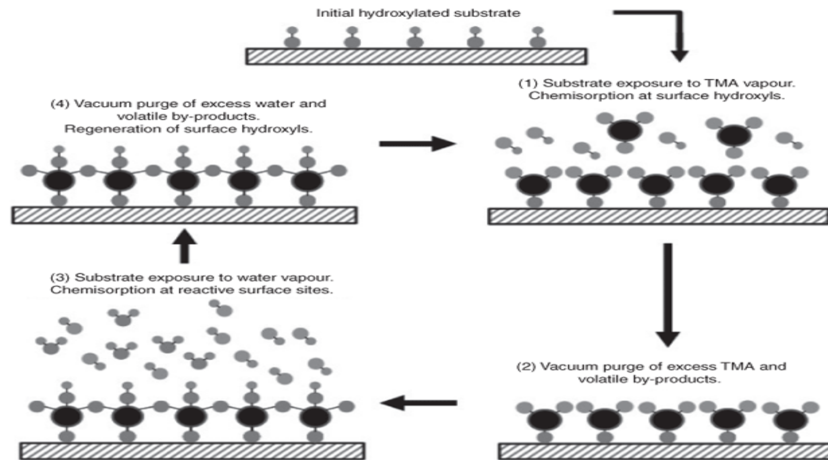

Figure 2. Schematic representation of one atomic layer deposition (ALD) cycle of Al_2O_3 growth using trimethylaluminium (TMA) and water. (Adopted from [8])

The surface chemistry for this reaction can be represented by the following half-step reactions:

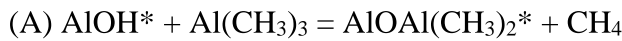

(A) $AlOH^* + Al(CH_3)_3 = AlOAl(CH_3)_2^* + CH_4$

(B) $AlCH_3^* + H_2O = AlOH^* + CH_4$

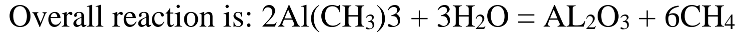

Overall reaction is: $2Al(CH_3)3 + 3H_2O = AL_2O_3 + 6CH_4$

The growth of the film occurs due to alternation of TMA and H_2O fluxes. Firstly, TMA is introduced to deposition chamber the it reacts with substrate, more specifically with substrate Al-O-H bonds, it can be said that these bonds are main drivers of the reaction. After formation of Al-O-Al-CH_3 connections, the excess of the reactant and CH_4 is purged with non-reacting gas (such as N_2). The next precursor is introduced shortly after, where now H2O reacts with Al-O-Al-CH_3 and form Al-O-Al-O-H structure, and again the excess of the reactant and CH_4 is purged. This cycle when reaped until full growth process is completed.

For information about ALD techniques variations check appendix. [7.2]

2.2 Importance of ALD and its applications

ALD has become one of the most versatile and frequently applied techniques for depositing thin films in the fields of in microelectronics, optics, biomedical engineering and nanotechnology. This is due to its ability to achieve atomic-level precision, which makes it ideal for creating high-quality dielectric materials for memory devices. ALD

plays a crucial role in the deposition of dielectrics for trench capacitors, significantly enhancing the performance and reliability of devices such as DRAMs, MRAMs, FeRAMs, RRAMs, and flash memories [1, 7-14], by providing control over the thickness of dielectric layers. The success of ALD can be attributed to its ability to produce uniformity and conformality, which are essential for optimizing electrical properties. Beyond memory devices, ALD has found widespread adoption in display technologies such as LCDs, OLEDs and other flat-panel displays [15]. ALD-deposited thin films contribute to the improved performance and longevity of these displays by enhancing properties such as light transmission, electrical conductivity, and barrier protection against environmental factors. In the field of photovoltaics, these films are used to deposit buffer layers, that are crucial for maintaining efficient charge carrier transport, reduce losses and act as protective coatings for solar cells. Additionally, ALD contributes to anti-reflection coatings, enhancing the absorption of sunlight to maximize energy conversion efficiency [16-17], by enhancing absorption of sunlight. These films not only improve the efficiency and stability of solar cells but also contribute to long-term reliability. Furthermore, ALD has revolutionized the development of advanced energy storage devices, including lithium-ion batteries, supercapacitors, and fuel cells [9-17]. By enabling the deposition of thin and uniform electrode materials and solid electrolytes, ALD enhances the energy density, cycling stability, and overall performance of these devices. This has driven advancements in portable electronics and renewable energy systems, as well as other fields that rely on efficient energy storage. In addition to its use in electronic and energy applications, atomic layer deposition (ALD) is also utilized in packaging technology to create thin barrier films that help prevent the diffusion or penetration of gases and moisture. These films extend the lifespan and reliability of electronic devices [18-19], by protecting sensitive components from degradation and corrosion caused by the environmental factors. ALD barrier films also play a role in food packaging, preventing microbial proliferation and enhancing the safety and shelf life of food products, by blocking the growth of bacteria [20-21]. This is particularly important in preserving food products against critical concerns, such as bacterial growth. Lastly, ALD has promising potential in biomedical engineering, particularly for surface modification of implants providing microbiostatic and biocompatible coatings to ensure patients safety. Additionally, it can be performed at relatively low temperatures, making it suitable for coating temperature-sensitive materials such as polymers. This allows for the surface modification of a wide range of materials without compromising their

mechanical or structural integrity. The coatings deposited by ALD exhibit excellent adhesion and stability over time, even under harsh conditions, ensuring the durability and reliability of biomedical devices and reducing the need for frequent replacements or revisions [22-23].

2.3 Factors affecting thin film growth

Understanding the properties and characteristics of thin films is essential for optimizing their performance across diverse applications. Various factors, including film structure, material composition, deposition technique or rate, pressure, temperature, defects, stress, and growth dynamics influence thin film properties, including mechanical, optical, electrical, thermal behaviour crystallographic structure and orientation [1, 7, 24]. Deposition technique plays crucial role in controlling film thickness, uniformity, and conformity. Choice between CVD, PVD and ALD may have their advantages and disadvantages.

ALD base reactions rely on self-limiting surface reactions to deposit thin films layer by layer in cycle manner, while CVD reactions are not. The deposition process in CVD is influenced by both gas-phase chemistry, mass transport and surface interactions. Deposition occurs in continuous introduction way, making it more complex than self-limiting process, which make achievement of uniformity harder in comparison to ALD. In contrast, PVD relies primarily on physical processes such as evaporation or sputtering (bombardment of energetic particles) of growth material to deposit material onto the substrate surface (Figure 3). PVD still involves controlling various parameters for film deposition, it typically does not involve the same level of chemical reactions or gas-phase chemistry as CVD, which simplifies the process.

While all three techniques involve controlling various parameters for film deposition, CVD typically relies on a broader range of factors due to its dependence on both chemical reactions and physical processes. PVD primarily rely on physical mechanisms for film deposition, while ALD offers control through self-limiting surface reactions. PVD can produce relatively uniform films over flat surfaces, but it may struggle to deposit uniformly on complex geometries or surfaces with high aspect ratios [24]. Overall, ALD's self-limiting nature and conformal coating capabilities make it well-suited for producing highly uniform thin films, particularly on complex surfaces or structures. However, PVD

remains a valuable technique for certain applications where high precision at the atomic scale is not required, and where other factors such as deposition rate or material properties are prioritized. All three techniques dictate the way how the adsorbed atoms are integrated into the growing process determine the final morphology of thin films, which may lead to different growth models.

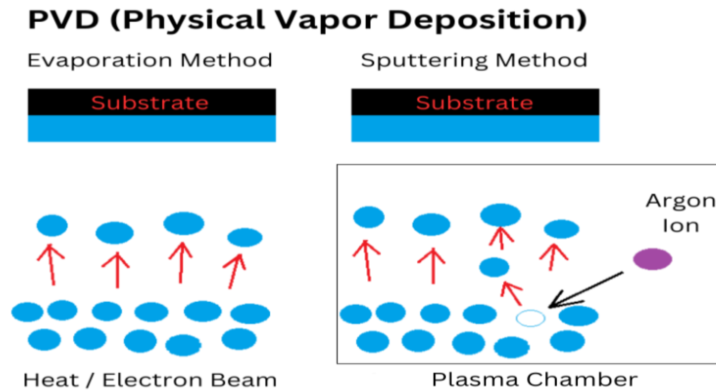

Figure 3. PVD Evaporation and Sputtering methods.

2.3.1 Growth models

Main growth models for thin films depositions are Frank van de Merve, Stranski-Krastanov and Volmer-Weber.

Volmer-Weber growth mode, islands or clusters of material nucleate randomly on the substrate surface, without forming a continuous film. This growth mode is typically observed when the adatom diffusion rate on the substrate surface is low relative to the deposition rate. The resultant film exhibits a rough and non-uniform surface morphology, with discontinuous islands or clusters dispersed across the substrate. While this growth mode may result in increased surface roughness and defect density, it can also offer unique properties, such as enhanced surface area and tuneable porosity (Figure 4) [25-26].

In this case of Frank van de Merve model atoms and molecules absorb directly onto the substrate surface and form continuous, uniform layer. This epitaxial growth mode is characterized by a smooth and flat film surface. The resulted layer-by-layer growth provides high crystalline quality and uniform thickness, making it suitable for applications demanding precise control and smooth interfaces (Figure 4) [27].

Stranski-Krastanov growth mode involves an initial layer-by-layer deposition followed by the formation of three-dimensional islands due to strain or lattice mismatch between the film and a substrate. Islands may nucleate and coalesce to form larger structures, leading to a mixed morphology comprising both flat regions and three-dimensional features. This growth mode often results in higher surface roughness, surface area, and increased defect density, which can be advantageous for applications requiring specific surface functionalities (Figure 4) [25-26].

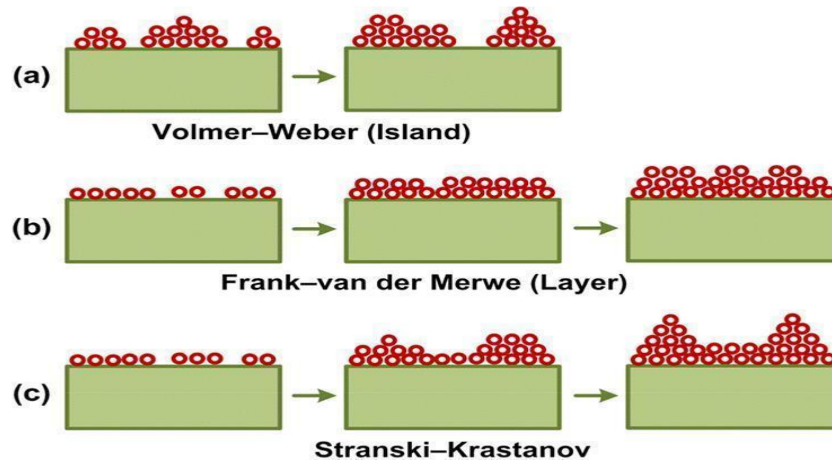

Figure 4. Different thin film growth mechanisms. (a) island growth model, (b) the layer-by-layer model, and (C) the mixed growth model. (Adopted from [25])

This growth models dictate the growth mechanisms and resulting film morphology, highlighting the importance of precise control during the ALD process [27]. Each deposition technique can result in this thin film growth models, but some tendencies can be assumed. ALD mostly result in Frank van de Merve growth model due to its sequential, self-limiting nature, but in some situation can promote Stranski-Krastanov model. CVD and PVD could proceed through all 3 models, but if precursors and substrate temperatures enable controlled surface reactions, they can promote layer-by-layer growth similar to ALD.

2.3.2 Precursor selection

Precursor as well as substrate are crucial components in thin film deposition. Selection of this two will not only affect film composition and properties, but also affect overall process, especially surface reaction. It is preferred for surface reaction to be quick and irreversible, leading to fast growth saturation. The precursor must possess adequate volatility to facilitate its transportation to the deposition chamber and should not

decompose until molecules have reached and reacted with the sample surface. In certain scenarios, the options for available reactants pertinent to a specific element may be severely restricted or entirely absent, the availability or synthesis of both the reactant and counter-reactant is essential for depositing the desired material. Some precursors may be harmful and trigger undesired reactions, resulting in dangerous by-products that could potentially damage the substrate, growing film or the ALD reactor itself. Moreover, the choice of reactants can be dictated by economic reasons, due to fact that some reactants are expensive and synthesis of them can be time consuming [3, 28]. Prior to deposition, thorough research of precursor availability and its reaction pathways is essential. It is vital to acknowledge that while ALD offers the potential for depositing substantial amounts of material, it is not universally applicable. Certain limitations must be recognized, not all materials can be grown using this method. Tables of materials has been grown by ALD are present in Table 1 [3]. This way we face the fact that perfect precursors don't exist, and the choice of precursor is usually a bargain between cost, availability, safety, volatility and reactivity.

Table 1. List of materials grown by ALD [3]

Elementa	Oxides	Nitrides	Sulfides	Other compounds
C, Al, Si, Ti, Fe, Co, Ni, Cu, Zn, Ga, Ge, Mo, Ru, Rh, Pd, Ag, Ta, W, Os, Ir, Pt	Li, Be, B, Mg, Al, Si, P, Ca, Sc, Ti, V, Cr, Mn, Fe, Co, Ni, Cu, Zn, Ga, Ge, Sr, Y, Zr, Nb, Ru, Rh, Pd, In, Sn, Sb, Ba, La, Ce, Pr, Nd, Sm, Eu, Gd, Tb, Dy, Ho, Er, Tm, Yb, Lu, Hf, W, Ir, Pt, Pb, Bi	B, Al, Si, Ti, Cu, Ga, Zr, Nb, Mo, In, Hf, Ta, W	Ca, Ti, Mn, Cu, Zn, Sr, Y, Cd, In, Sn, Sb, Ba, La, W	Li, B, Mg, Al, Si, P, Ca, Ti, Cr, Mn, Co, Cu, Zn, Ga, Ge, As, Sr, Y, Cd, In, Sb, Te, Ba, La, Pr, Nd, Lu, Hf, Ta, W, Bi

2.3.3 ALD Window

At some specific conditions, the ALD-type of deposition reactions may not exhibit self-limiting behaviour and one of these conditions is ALD window (Figure 5) [29]. The temperature window is the range of deposition temperatures within which the growth rate is self-limiting, uniform, and consistent, resulting in thin films with desired properties such as uniform thickness, high conformality, minimal defects, precise stoichiometry, and strong adhesion to the substrate. Deposition outside the ALD window usually results in non-uniform, poor quality and growth rate, with possibly for reactions to exhibit non-self-limiting nature. The reasons behind it can be neither too low or high temperature outside deposition window, where high temperature results in thermal decomposition or rapid desorption of the precursor and low temperature in slow reaction kinetics or precursor condensation [2-3, 7, 28-29]. This way the ALD temperature window is crucial condition, which is very important factor to research for each precursor, to minimize the possibility of fault depositions and ensures desired properties of thin film.

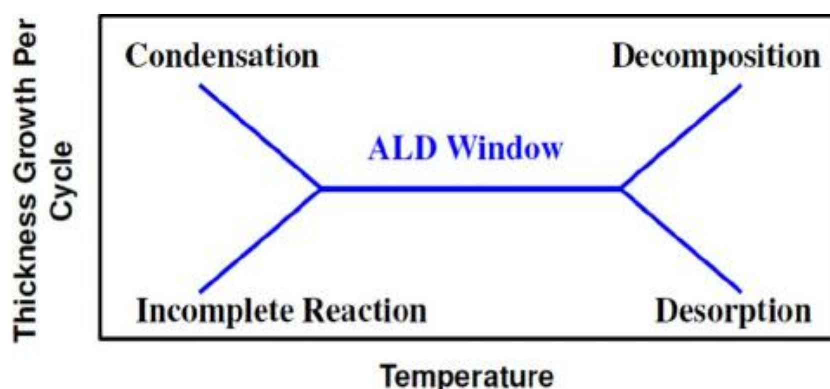

Figure 5. Model of ALD window. (Adopted from [29])

2.3.4 Pulse length and ALD cycles

In atomic layer deposition (ALD), pulse length refers to the time allocated for the introduction of precursor molecules into the reaction chamber or for purging with an inert gas. This process is essential for controlling the growth and properties of thin films [2-3]. The related concept of precursor dose is critical to understanding ALD processes, as it represents the amount of precursor molecules delivered to the substrate surface during the pulse. Pulse length and precursor dose are interrelated, as the dose depends not only on the pulse duration but also on factors like precursor pressure and flow rate.

The primary goal of the precursor pulse is to achieve surface saturation, a state where the substrate surface is fully covered by a single monolayer of precursor molecules without overloading it. The pulse length must be sufficient to deliver the required dose for saturation. In most ALD systems, the required time for this depends on the precursor's reactivity, vapor pressure, and the reactor design. While longer pulse times may increase the precursor dose, leading to potentially higher growth per cycle, excessively long pulse durations can oversaturate the surface and disrupt the self-limiting nature of the ALD process, causing non-ideal film growth. For example, in some reactors, saturation may be achieved within fractions of a second, while others may require several seconds depending on system conditions. This emphasizes the importance of setting up the pulse length to the specific precursor and reactor system to ensure uniform and controlled growth.

The purge pulse on the other hand involves introducing an inert gas (commonly nitrogen or argon) to remove excess precursor molecules and reaction by-products before introducing the next reactant. Sufficient purge time is critical to preventing unwanted side reactions and ensuring the self-limiting nature of ALD. While longer purge times enhance the removal of excess species, excessively long purge durations reduce throughput without significantly improving film quality in many cases. Thus, optimizing purge times balances effective removal with overall process efficiency.

The ALD cycle number refers to the number of times the precursor pulse-purge sequence is repeated to achieve the desired film thickness. Longer precursor pulse times with multiple cycles can lead to thicker films, but they may also increase the risk of defects or surface roughness due to imperfections accumulating over successive layers. Therefore, selecting the appropriate cycle count and pulse lengths requires consideration of the film's application-specific requirements, such as uniformity, thickness, and functional properties. In summary, the precursor pulse length, dose, purge duration, and cycle number are all interconnected parameters that determine the quality and characteristics of ALD thin films. Careful optimization of these variables is essential for achieving precise, uniform, and defect-free film deposition tailored to the desired application.

2.4 SiO_2 literature review

2.4.1 Deposition techniques and precursors

The choice of deposition technique has a significant impact on the quality, difficulty, and cost of thin film fabrication. SiO_2 can be deposited using both chemical and physical methods. However, due to the increasing demand for uniform thin films in various fields such as electronics, optics, and packaging, there has been a preference for using chemical self-limiting reactions for deposition. This preference makes Atomic Layer Deposition (ALD) and Chemical Vapor Deposition (CVD) well-suited for SiO_2 deposition purposes [1-4, 7]. Most silicon precursors fall into the category of organosilicons, encompassing silanes, cyanates, halides, oxygen-containing compounds, amines, or heterocycles. These precursors can be classified into three groups, as shown in Table 2 [30-31].

Silanes are organic compounds containing silicon and hydrogen atoms. They are valued for their ability to form strong Si-O bonds, which are essential for the creation of SiO_2 thin films. In addition to the potential for forming high-purity products due to the simplicity of the molecule and the absence of complex by-products. Moreover, silanes are also highly reactive compounds which are exhibiting a highly pyrophoric properties that are posing a significant safety hazard, as they can ignite spontaneously when exposed to air. Consequently, these precursors require strict handling and specific storage conditions to prevent accidents [30-35].

Alternative to silane became organo-silicon precursors like: $C_4H_{12}Si$ (TMS), $C_8H_{20}O_4Si$ (TEOS) (oxygen-containing), $C_8H_{24}N_4Si$ (TEAS) (aminosilanes), $C_9H_{23}NO_3Si$ (APTES) (cyanates) or $SiCl_4$ (silicon halides) [30-35]. Organosilicons contain organic groups bonded to silicon atoms and may contain elements like oxygen, nitrogen or both, while silicon halides may contain only halide atom or with organic group. These substitutes offer not only chemical stability making in the most cases easier to handle these precursors at room temperature, but also tunability in film properties due to the organic functional groups and a wide range precursors availability, allowing for process customization based on specific deposition requirements (temperatures, properties, composition).

Table 2. SiO2 precursors examples Table 2 [30-31]

H (Silanes)	H, C (Organosilicon)	H, C, Group V (Aminosilanes)	H, C, Group VI	H, C, Group VII
SiH_4	$C_4H_{12}Si$ (TMS)	C_4H_9NSi	$C_5H_{12}O_3Si$ (VTMOS)	SiH_3Cl
Si_2H_6	$C_5H_{10}Si$	$C_5H_{14}SiN$	$C_5H_{14}OSi$	SiH_2Cl_2 (DCS)
Si_3H_8	$C_6H_{14}Si$	$C_5H_{15}NSi$ (DMATMS)	$C_6H_{16}O_3Si$	$SiHCl_3$
	$C_6H_{16}Si$ (TES)	$C_6H_{12}N_2Si$	$C_6H_{18}OSi_2$	$SiCl_4$
	$C_6H_{18}Si_2$	$C_6H_{16}N_2Si$ (BEMAS)	$C_7H_{12}OSi$ (TVMOS)	Si_2Cl_6
	$C_8H_{18}Si_2$	$C_6H_{17}NSi$ (DIPAS)	$C_8H_{20}O_4Si$ (TEOS)	SiH_3F
	$C_8H_{20}Si$	$C_6H_{18}N_3Si$ (TDMAS)	$C_9H_{14}O_3Si$	SiH_2F_2
	$C_9H_{14}Si$	$C_6H_{18}N_2Si$ (BDMAS)	$C_9H_{18}OSi$	$SiHF_3$
	$C_{10}H_{10}Si$	$C_6H_{19}N_3Si$	$C_9H_{23}NO_3Si$ (APTES)	SiF_4
	$C_{10}H_{16}Si$	C_7H_9NSi	$Si(NCO)_4$ (TICS)	Si_2F_6
	$C_{12}H_{12}Si$	$C_8H_{21}NSi$ (DSBAS)	$C_{12}H_{12}O_2Si$	SiH_3Br
	$C_{14}H_{14}Si$	$C_8H_{22}N_2Si$ (BTBAS)	$C_{14}H_{16}O_2Si$	SiH_2Br_2
	$C_{15}H_{15}Si$	$C_8H_{24}N_4Si$ (TEAS)	$C_{18}H_{16}OSi$	$SiHBr_3$
	$C_{16}H_{16}Si$	$C_{10}H_{21}N_2Si$	$C_{12}H_{28}O_4Si$ (TBS)	$SiBr_4$
	$C_{17}H_{16}Si$	$C_{10}H_{22}N_2Si$	$C_{15}H_{34}O_4Si$ (TPS)	SiH_3I
	$C_{18}H_{16}Si$	$C_{12}H_{32}N_2Si_2$ (BDIPADS)		SiH_2I_2
		$C_{12}H_{36}N_6Si_2$ (AHEAD)		$SiHI_3$
				SiI_4
				Si_2I_6
				CH_2Cl_4Si
				CH_3Cl_3Si
				$C_2H_6Cl_2Si$

However, these precursors often decompose into complex by-products if they don't have simple structure, which can affect film purity due to organic or nitrogen components. Precursor synthesis or availability may be complex or expensive (e.g., cyanates). Also, sometimes even by-products of these reaction may be toxic or damage reactor/substrate. Therefore, management, knowledge and precise control of reaction pathway is curial while exploitation of these precursors.

Additional information about SiO_2 application in electronics and optics can be found appendix. [7.3]

2.4.2 Silicon oxide deposition from hexakis(ethylamino)disilane

In this work, it was chosen to deposit a SiO_2 film using the T-ALD process and one of the aminosilanes group precursors, more specifically, hexakis(ethylamino)disilane, sometimes abbreviated as AHEAD ($Si_2(NHEt)_6$) due to the properties of AHEAD and previously published data on it [36-41]. Ozone (O_3) was chosen as the most reliable and well-working oxygen source.

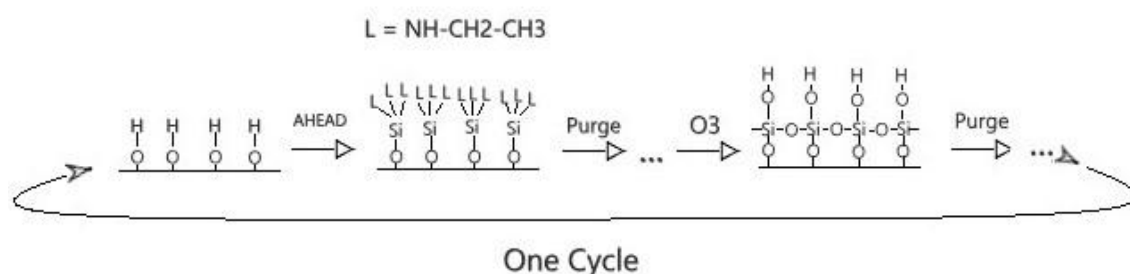

Figure 6. AHEAD + O_3 cycle.

Surface chemistry of AHEAD + O_3 precursors on silicon substrate can be summarized on Figure 6. $Si_2(NHEt)_6$ is introduced first, then the process is followed by silicon atom exchanging one or several of its ligands with the hydroxylated surface, -OH groups. After that three alternative reaction paths can take place (Figure 7).

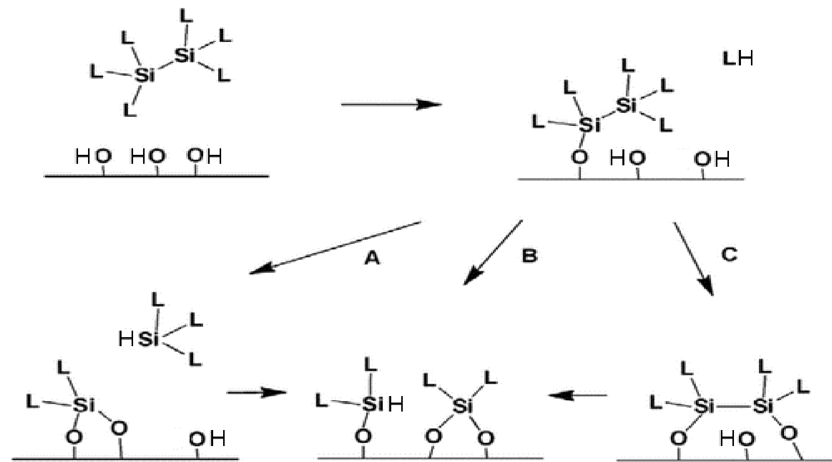

Figure 7. Schematics of possible reaction pathways for the attachment of $Si_2(NHEt)_6$ on a hydroxylated surface. (Based on graph from [40]).

One of option is that hexakis(ethylamino)disilane species will react a neighbouring −OH group and this way remove one silicon part in the gas phase, path A (Figure 7). There is also a possibility of chemisorption of full AHEAD species from reaction with -OH group, resulting in one containing Si-H bond, path B (Figure 7). The chance of both Si centres sticking to the surface by exchanging one or more of their ligands, while maintaining the Si-Si bond intact can also be possible, path C (Figure 7). All these three reactions possible but mostly will lead to (path B) (Figure 7) or just Si-O-Si-L_3 structure. Later, when the first precursor introduction has been completed, a purge step with an inert gas (N_2) takes place, removing excess precursors and reaction by-products, which are mostly $CH_3CH_2NH_2$ (ethylamine). The third part of the reaction can be considered as the O_3 pulse precursor introduction. Ozone molecules eliminate the remaining ligands by forming CH3CHO (acetaldehyde), remove SiH bond via H_2O formation, connect Si atoms by Si-O-Si bond and regenerate the Si–OH groups. Shortly after the last purge pulse, the reactor is cleaned again from reaction products and O_3, making it possible to repeat the reaction and deposit the next SiO_2 layer.

3 Characterization of silicon oxide films

The thickness and compositional properties of the silicon oxide films were measured using ellipsometry for Si substrates and X-ray fluorescence (XRF) for Mo samples. These measurements provided information about the film's uniformity and elemental composition. All measurements and calculations were performed using the respective

instruments, and the data analysis was conducted with the manufacturer-provided software.

3.1 Ellipsometry

Ellipsometry is a powerful optical technique used to characterize materials and thin films by analysing the differences in amplitudes and phases of light waves reflected or transmitted from the surface under investigation. At its core, ellipsometry relies on the polarization of light, which is the orientation of the electric field vector with respect to the direction of propagation (Figure 8) [42-43]. When unpolarized light interacts with a surface, its behaviour changes depending on the angles between the surface normal, the direction of light propagation, and the electric vector. By measuring these changes, ellipsometry provides valuable information about the optical properties of the material, such as refractive index, absorption coefficient, and film thickness [42-46]. One of the key applications of ellipsometry is in measuring thin film thickness. When light interacts with a thin film on a substrate, multiple reflections occur within the film leading to interference effects that depend on the film thickness. By analysing the changes in polarization caused by these interference effects, ellipsometry can accurately determine the thickness of thin films (Figure 9) [42-46].

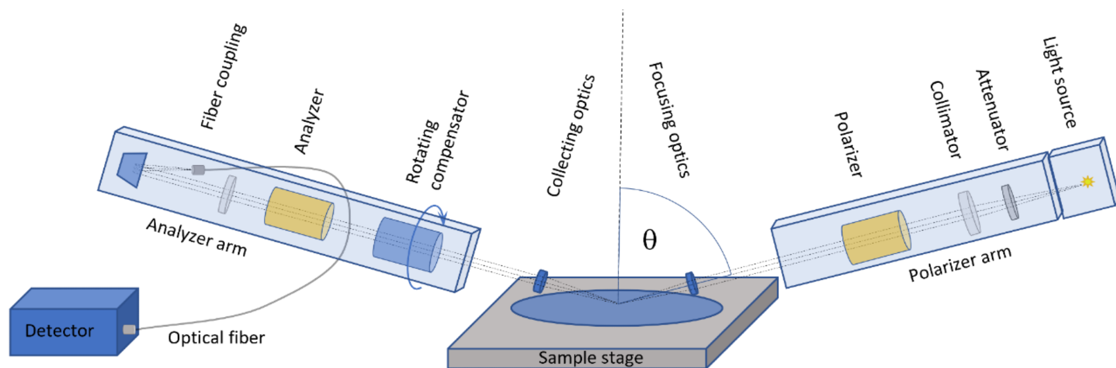

Figure 8. Schematic of ellipsometry scanner. (Adopted from [42])

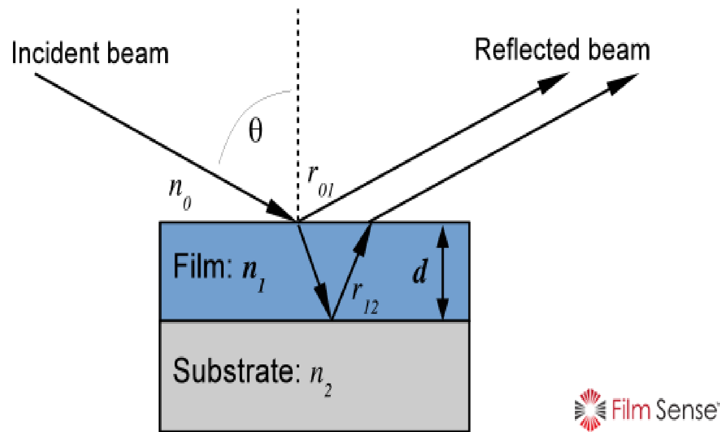

Figure 9. Thin film thickness measurement. (Adopted from [44])

The change in polarization state caused by the sample reflection can be defined by the ratio of the sample reflectivity for p-polarized light (R_p) (Y axis) (parallel to the plane of incidence), over the sample reflectivity for s-polarized light (R_s) (X axis) (perpendicular to plane) (Figure 10).

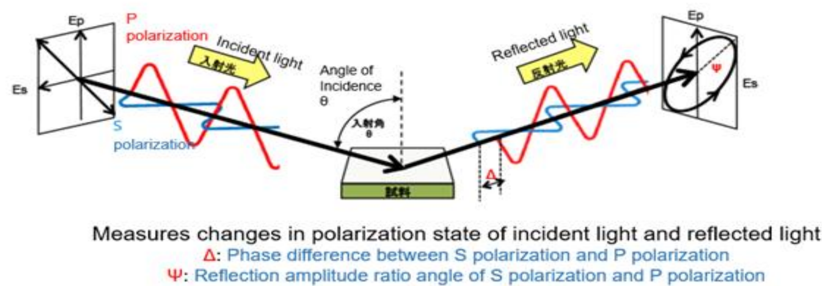

Figure 10. Polarization of light. (Adopted from [43])

This ratio is a complex number, which is typically denoted by ρ (rho), and is often reported in terms of the ellipsometric parameters Ψ (Psi) and Δ (Delta), as defined by the following complex number equation (1) [44].

$$\rho = \frac{Rp}{Rs} = \tan \Psi \, e^{i \cdot \Delta} \quad (1)$$

According to this equation, tan(Ψ) defines the magnitude of the reflectivity ratio for p- and s- polarized light, and Δ defines the phase difference between the reflected p- and s-

polarized light. Ellipsometry, measuring both Ψ (Psi) and Δ (Delta), allows for the direct determination of two sample-related parameters: the film thickness (d) and the film's refractive index (n_1). This is achieved through numerical inversion of the thin film interference equation depicted in correlations between equations (2). Here, the reflection coefficients $R_{p,s}$ at each interface and the film phase factor β are computed utilizing the refractive index of each medium, the angle of incidence (θ), the Fresnel equations, and Snell's law [44]. All these calculations were performed using specialized software and example of ellipsometer used can be seen on Figure 11 [46].

$$\rho = \tan\Psi\, e^{i\cdot\Delta} = \frac{Rp}{Rs} = \frac{\dfrac{r_{p01} + r_{p12}e^{-i2\beta}}{1 + r_{p01}r_{p12}e^{-i2\beta}}}{\dfrac{r_{s01} + r_{s12}e^{-i2\beta}}{1 + r_{s01}r_{s12}e^{-i2\beta}}} \quad \beta = 2\pi\frac{d}{\lambda}n_1\cos\theta 1 \qquad (2)$$

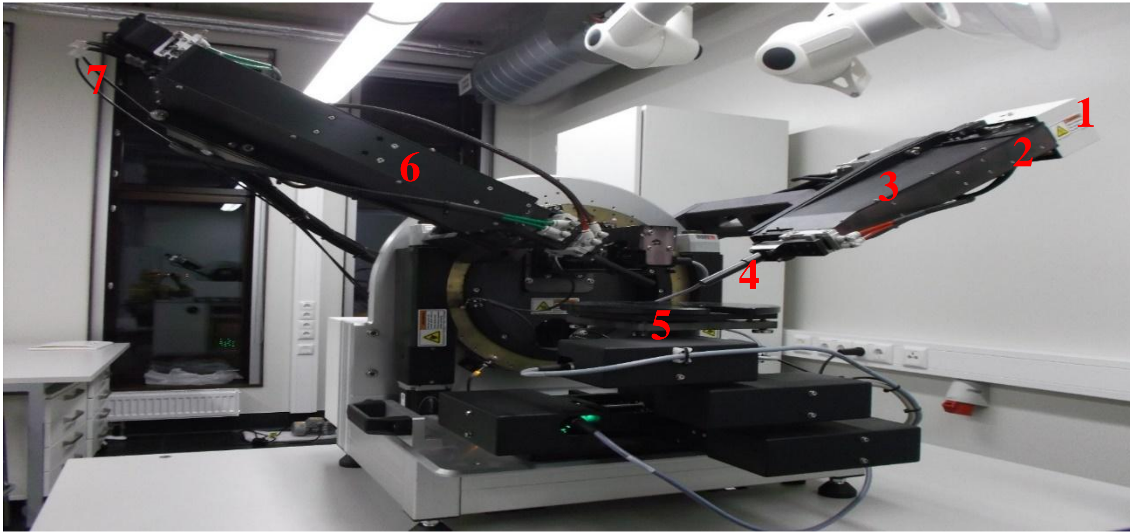

Figure 11. Measuring part of the ellipsometer GES-5E. 1 – Xe-lamp, 2 – neutral filters (inside a shoulder), 3 – polarizer (inside a shoulder), 4 – telescope for incident light, 5 – object stage, 6 – analyser (inside a shoulder), 7 – signal fibers.

3.2 XRF

X-rays are a form of electromagnetic radiation characterized by their high energy and their short wavelengths (0.01 to 10 nm) [47], positioned in the spectrum between gamma rays and ultraviolet radiation (Figure 12). Unlike electromagnetic waves with longer wavelengths, X-rays can penetrate materials due to their relatively low absorption coefficients in many substances. The extent of penetration depends on the atomic number

and density of the material; materials with lower atomic numbers and lower density generally allow X-rays to penetrate deeper due to reduced absorption and scattering.

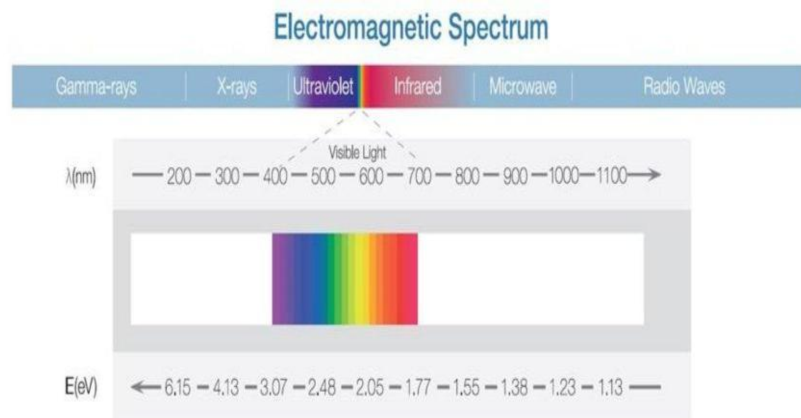

Figure 12. Electromagnetic Spectrum. (Adopted from [47])

X-rays are generated using an X-ray tube, which consists of an anode (anti-cathode) and a cathode connected by a high-voltage circuit (Figure 13) [47-49]. When this high voltage is applied, electrons are accelerated from the cathode and directed towards the anode. Upon striking the anode, the kinetic energy of the electrons is converted into X-ray photons.

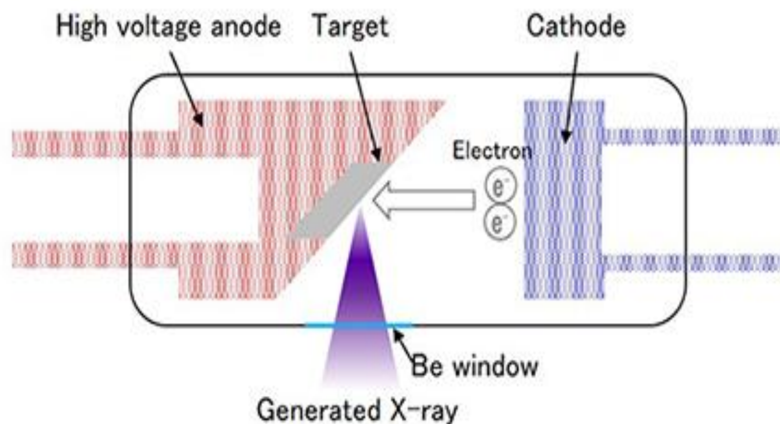

Figure 13. X-ray tube. (Adopted from [48])

As the X-rays penetrate the sample, they interact with the atoms present. Some of the X-rays are absorbed by the atoms in the sample, causing inner-shell electrons to be knocked out of their orbits (Figure 14) [47]. This creates vacancies in the inner electron shells (K shell, L shell, M shell) [47-49], leading to higher energy, unstable configurations for the

atoms. Electrons from outer shells then transition to fill these vacancies. As outer-shell electrons transition to lower energy levels, excess energy is emitted in the form of characteristic fluorescent X-rays. Each chemical element has a unique arrangement of electrons in its orbitals, leading to characteristic energy levels for each element. Consequently, the energy of the emitted X-rays serves as a distinctive “fingerprint” for identifying the elements present in the sample.

There are two main types of XRF detectors: energy-dispersive XRF (EDXRF) and wavelength-dispersive XRF (WDXRF) (Figure 15) [48]. In the wavelength-dispersive X-ray fluorescence (WDXRF) setup, the emitted X-rays from the sample are dispersed according to their wavelengths using a solar slit and dispersive crystal. The solar slit helps to narrow down the incoming X-ray beam, while the dispersive crystal separates the X-rays based on their wavelengths [47-49]. The more complex system structure allows precise separation of X-rays with different energies, more preferable for complex samples where precise measurement and reduced spectral overlaps are crucial.

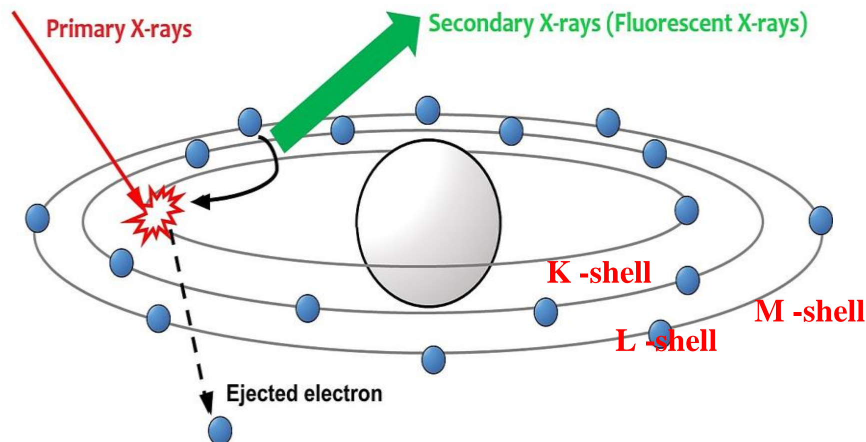

Figure 14. Principle of Fluorescent X-rays Emission. (Adopted from [47])

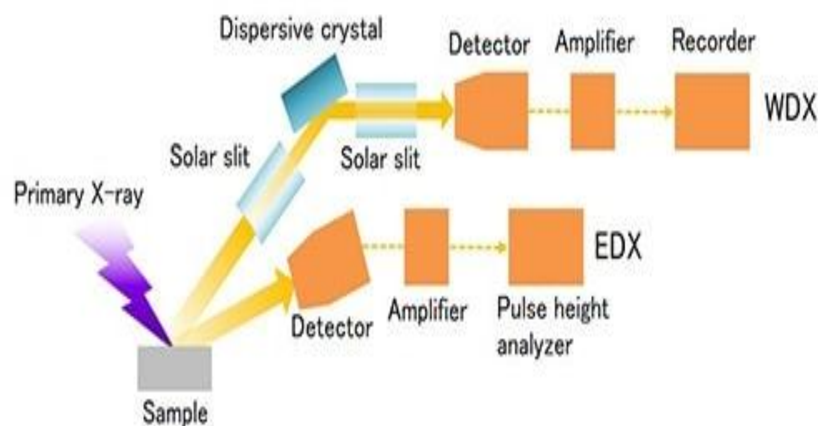

Figure 15. WDX and EDX types of instruments. (Adopted from [48])

On the other hand, the detector in EDX directly measures the energies of the emitted X-rays from the sample. These detectors typically use semiconductor materials such as silicon (Si) or germanium (Ge). When an X-ray photon strikes the detector, it generates electron-hole pairs within the semiconductor material. The resulting electrical signal is proportional to the energy of the incident X-ray photon [47-49]. EDX has good energy resolution and requires no dispersion system, which allows the instrument to be smaller in size. Widely used for routine elemental analysis in various fields such as mining, cement, petrochemicals, and environmental analysis.

4 Experiment set-up

To evaluate the distribution of film deposition along the substrate holder and within the deposition chamber, five substrate pieces were used for each experiment. This arrangement allowed for the collection of a large amount of statistical data for each growth parameter change, verification of reproducibility and consistency across depositions, and minimized time consumption compared to depositing samples individually. The substrates included five silicon (Si) pieces and five molybdenum (Mo) pieces, arranged on a substrate holder approximately 10.8 cm in length (Figure 16). Molybdenum samples were used in this work for XRF measurements due to the possible interference of silicon substrate with measurements of silicon/oxygen films, which may affect the measured composition. The substrates were spaced evenly along the holder to observe variations in film deposition across its length. Each sample was labelled from I to V for both substrate types, beginning at the narrower end of the holder and progressing toward the wider end. The first sample was positioned such that its midpoint aligned with

the 2 cm mark on the holder’s ruler. Subsequent samples were spaced 2 cm apart, measured from the midpoint of the preceding sample (Figure 16). The substrate holder's design, with a width tapering from approximately 3.2 cm at the narrow end to 3.33 cm at the wider end, created a slight slope when placed in the growth chamber. This sloped positioning improved the exposure of all substrates to the precursor molecules during deposition (Figure 17). Further details on the reactor setup are provided in the appendix. [7]

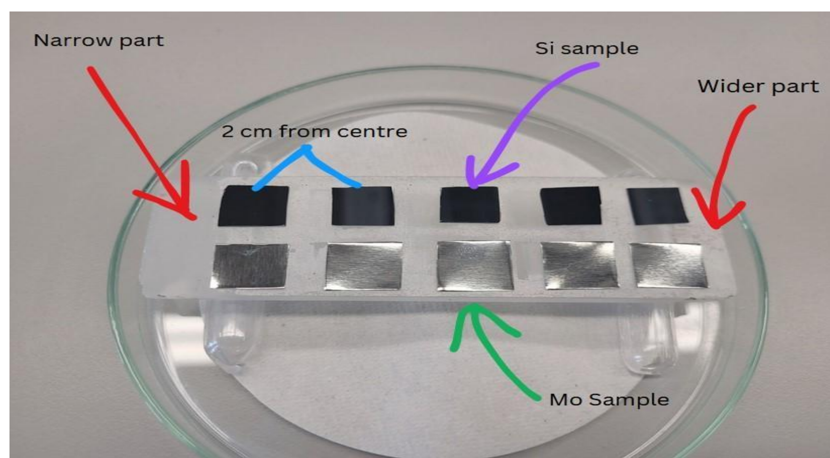

Figure 16. Substrate holder with substrate samples.

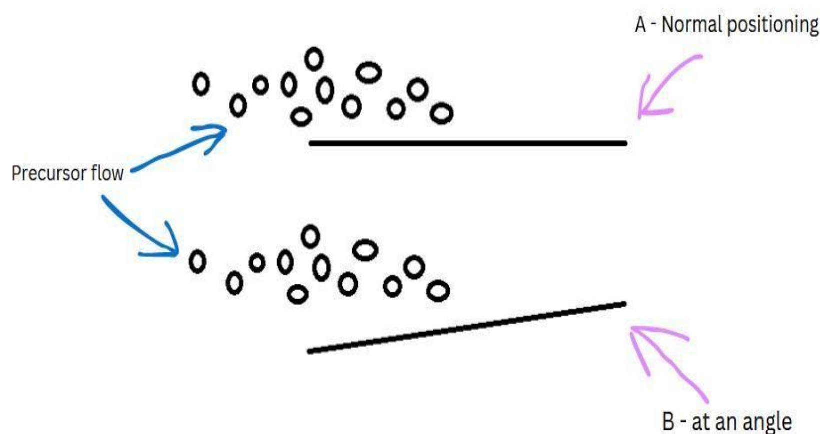

Figure 17. Substrate holder positioning in the reactor.

Four main parameters were changed: temperature inside growth and evaporation chamber, and pulse lengths for both AHEAD and ozone precursors. Pressure inside the reactor for all experiments was kept about ~2.11 mbar while ozone concentration varied between all depositions 253-262 g/Nm^3, but average value can be considered as ~256.1

g/Nm^3. The working temperature and pulse lengths were different for each individual experiment series.

To investigate the influence of temperature on the thickness of the thin film, it was decided to start the growth process at a temperature of 90°C and 120°C to see how the ozone and AHEAD precursors would behave in conditions with low temperatures, where reactivity may be slower. Every consequent deposition was performed with the temperature increase of 60°C until final value of 480°C was reached. All the temperature set points on the graphs presented were rounded for easier readability.

Considering the temperature change of growth and precursor evaporation, the cycle count was set to 1200 cycles. The precursors and purge pulses were the same: 2/2/5/5 seconds, where 2/2 seconds were for the AHEAD pulse/purge and 5/5 seconds for the ozone pulse/purge, respectively. The main changes were in temperature set up.

In case of AHEAD and ozone precursors, the relationship between precursor pulse and resulted film was studied. For these purposes the cycle count was set to 600 cycles, to increase experiments efficiency in terms of time and resources. With 600 cycles, there should be an adequate number of data points to draw meaningful conclusions about the effects of precursor pulse time variations. For temperature configuration it was chosen to set evaporation temperature to 60-61 °C as the most efficient (Figure 23) and 240-244 °C for growth process. The precursors pulses were changed for each deposition, but purge pulses were left unchanged, to reduce the complexity of the experimental design and data analysis.

5 Results and discussion

Next part of the work present results of XRF and ellipsometry measurements, which are described and analysed.

5.1 Deposition gradients and chemical compositions

In this chapter deposition gradients and chemical compositions at different growth temperatures are presented, based on XRF measurements.

5.1.1 Deposition gradients

Gradient is the difference between material amount deposited during one deposition between samples. XRF represents here total amount of oxygen and silicon in µg/cm2 units. Figure 18 shows that at growth temperatures 90 °C, 120 °C, 420 °C, 480 °C the resulted films have non-uniformity in total material amount across samples. At growth temperatures between 180-360 °C showed higher uniformity to each other.

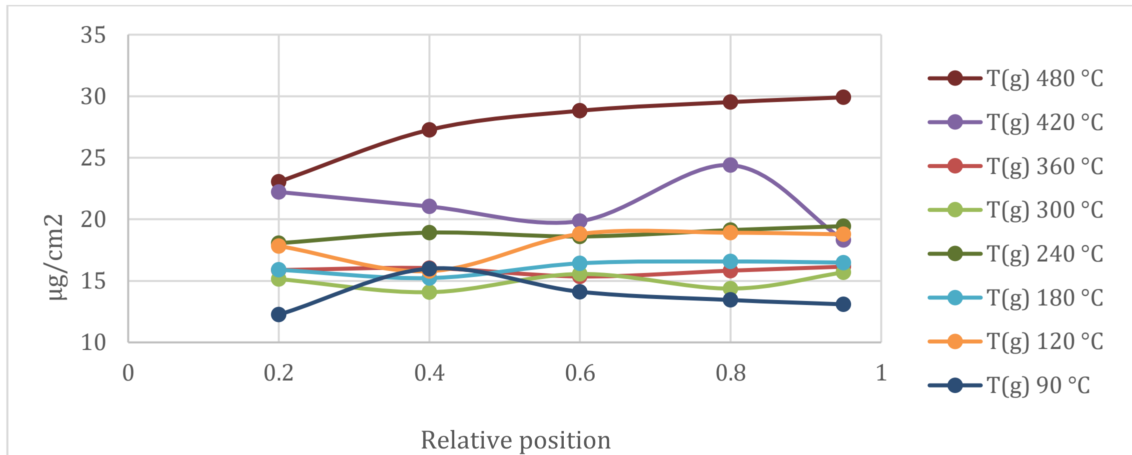

Figure 18. XRF of total amount of oxygen and silicon, dependence on growth temperature.

A different situation can be observed on Figure 19, where dependence on precursor evaporation temperature and amount of deposited material is presented. The AHEAD showed the best uniformity only for temperature set point of 60 °C, while other temperatures, lower or higher, didn't exhibit any uniform growth behaviour.

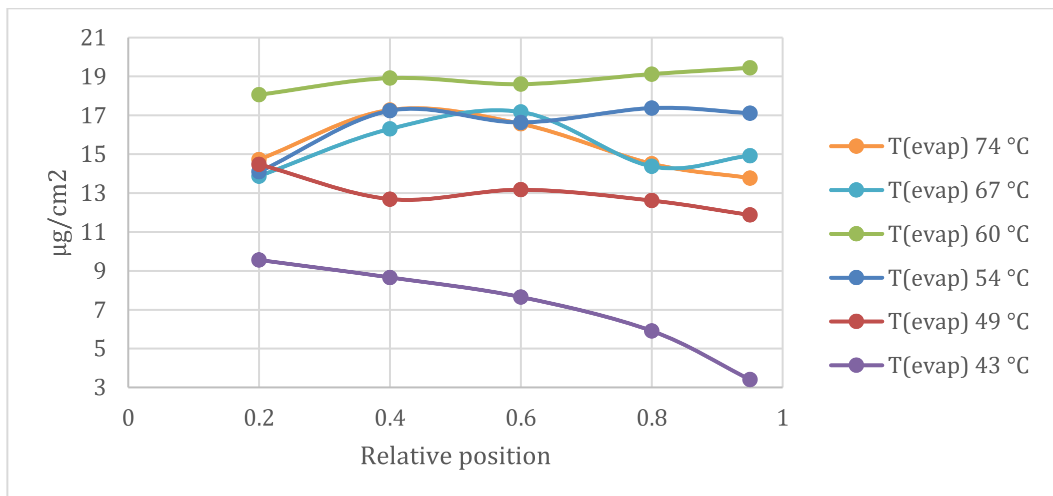

Figure 19. XRF of total amount of oxygen and silicon, dependence on precursor evaporation temperature.

A change in the length of the AHEAD precursor pulse led to a situation where all set points in time showed an inability to achieve close uniformity between samples (Figure 20). All experiments with an ozone pulse produced wave-like graph lines on Figure 21, which cannot be considered to represent high uniformity.

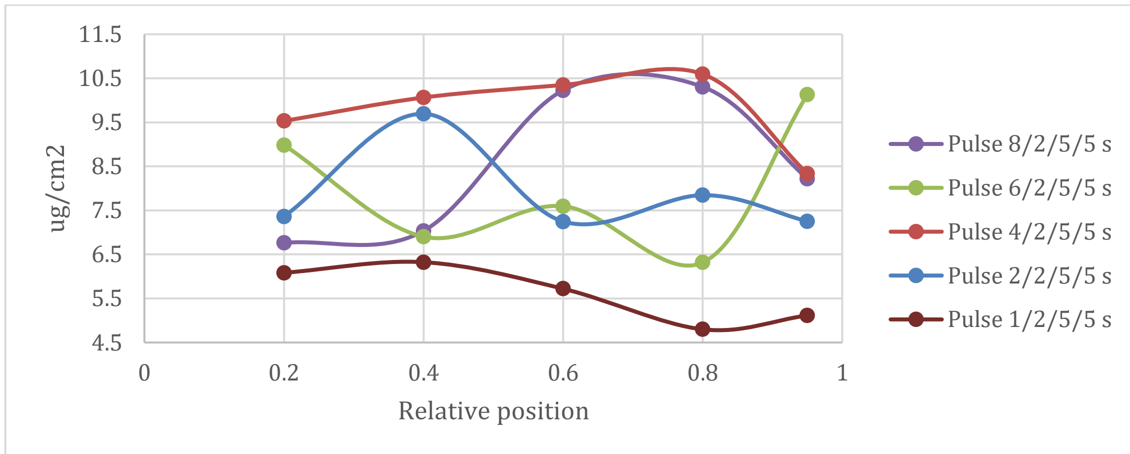

Figure 20. XRF of total amount of oxygen and silicon, dependence on AHEAD pulse.

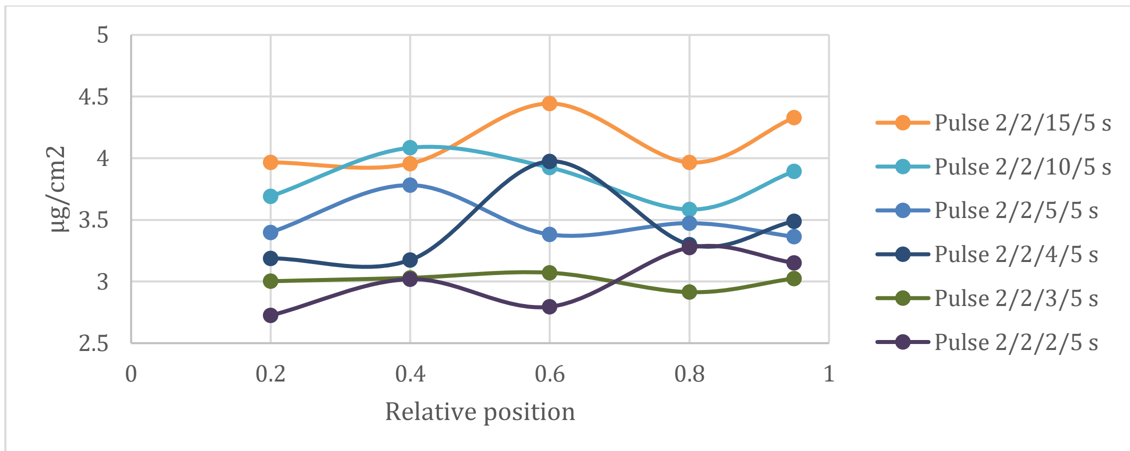

Figure 21. XRF of total amount of oxygen and silicon, dependence on ozone pulse.

5.1.2 Chemical composition

In general ratio of SiO_2 is 1/2 where for 1 atom of silicon there are 2 atoms of oxygen. The ratio calculation of oxygen and silicon from amount of material per area deposited will help to understand the overall chemical composition of film produced. For calculation of ratio the μg/cm^2 results of Si and O must be dived by molar masses, which will result in μmol/cm^2 from that the ratio between silicon and oxygen can be determined. Results from Table 3 suggest that the closest to original ratio can be produced at growth

temperatures 90 °C, 180 °C, 300 °C, 360 °C and 420 °C, while other mostly results in lower ratio. Temperatures like 240 °C and 480 °C have showed lowest results in ratio, while 480 °C may be too high temperature for this kind of precursor, 240 °C on the other hand may be explained by measurement error or unsuccessful deposition result.

Table 3. Amount of material per area results at different T(g) as measured by XRF.

	Average µg/cm^2		Average µmol/cm^2		Ratio
Temperature, °C	O	Si	O	Si	Si/O
480	16.15894	11.15428	1.010	0.398	0.394
420	11.86482	9.29976	0.742	0.332	0.448
360	8.20232	7.66792	0.513	0.274	0.534
300	7.48346	7.4842	0.468	0.267	0.571
240	10.866628	7.96384	0.679	0.284	0.419
180	8.274	7.82726	0.517	0.280	0.541
120	10.19212	7.83132	0.637	0.280	0.439
90	7.50538	6.27354	0.469	0.224	0.478

Regarding other results the change in precursor T(evap) the closest to original silicon dioxide ratio where depositions at 74 °C, 67 °C and 43 °C (Table 4), for AHEAD precursor pulse at 8/2/5/5s (Table 5) and for ozone pulse at 2/2/5/5 s (Table 6).

Table 4:. XRF, amount per area results for evaporation temperature series.

	Average µg/cm^2		Average µmol/cm^2		Ratio
Temperature, °C	O	Si	O	Si	Si/O
74	8.30898	7.0623	0.519	0.252	0.486
67	8.1845	7.1468	0.512	0.255	0.499
60	10.86628	7.96384	0.679	0.284	0.419
54	9.535375	6.8019	0.596	0.243	0.408
49	7.23866	5.7262	0.452	0.205	0.452
43	3.77904	3.2563	0.236	0.116	0.492

Table 5. XRF, amount per area results for AHEAD precursor pulse series.

	Average µg/cm^2		Average µmol/cm^2		Ratio
Time, s	Si	O	O	Si	Si/O
8/2/5/5	4.46702	4.04546	0.279	0.144	0.518
6/2/5/5	4.03624	3.95008	0.252	0.141	0.559
4/2/5/5	5.55662	4.21766	0.347	0.151	0.434
2/2/5/5	4.32418	3.47966	0.270	0.124	0.460
1/2/5/5	2.62572	2.98314	0.164	0.107	0.649

Table 6. XRF, amount per area results for ozone pulse series

	Average µg/cm2		Average µmol/cm^2		Ratio
Time, s	Si	O	O	Si	Si/O
2/2/15/5	4.07616	4.13236	0.255	0.148	0.579
2/2/10/5	4.15666	3.8355	0.260	0.137	0.527
2/2/5/5	4.32418	3.47966	0.270	0.124	0.460
2/2/4/5	3.23002	3.42554	0.202	0.122	0.606
2/2/3/5	2.9924	3.00864	0.187	0.107	0.575
2/2/2/5	3.4301	2.99314	0.214	0.107	0.499

5.2 Temperature dependence

5.2.1 Growth temperature influence on film thickness

The graph on Figure 22 shows the relationship between sample thin film thickness and T(g) is presented. Looking at these graphs more closely, at 120 °C and 180 °C temperatures the highest thickness results were achieved, 118,3 nm for 120 °C and 118.9 nm for 180 °C, respectively.

The other temperatures at the same time show a lower average thickness result and complicated growth behaviour. At temperature of 300 °C and 180 °C results showed the best similarity in thickness across all five substrates samples. In addition to that it can be noticed that thickness at 300 C° is higher than at 360 °C and almost equal to 420 °C; results of 90 °C are higher than 360 °C, but not uniform across samples; 90 °C and 240 °C have the most noticeable drop in thickness on one of their substrate samples.

One of possible explanation of this results may be measurements errors during measurement, for example object wasn't scanned properly or objects weren't large enough in size, which could explain drop in thickness for 90 °C and 240 °C temperatures. Second possibility may be that some samples the scratched during transfer or use. Other reasons may be found in the ALD process window.

If the temperature is between 120 °C and 180 °C, film deposition occurs within an optimal range. Depositing below this range can lead to thinner films due to unsaturation; while depositing above it may cause precursor decomposition and affect growth behaviour. However, most deposited films will still have relatively similar thicknesses, with some being slightly thicker than others.

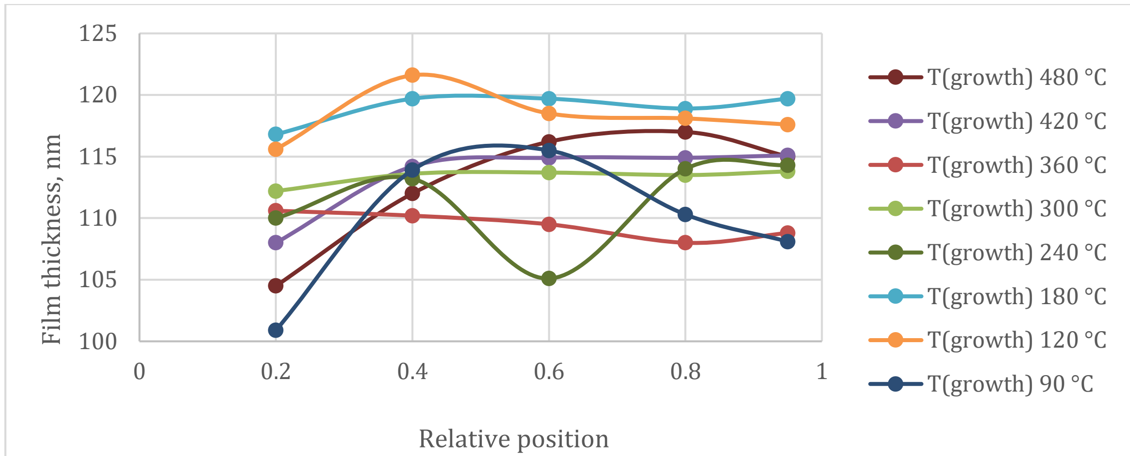

Figure 22. Ellipsometry measurements of Thickness vs T(g).

5.2.2 Precursor evaporation temperature

In case of precursor evaporation, we can see the following trend on Figure 23. The temperature of 60 °C is the most favourable for deposition with AHEAD precursor, resulting in the highest average thickness of 111.3 nm among all films. Deposits below this point, at 49 °C and 54 °C, showed results that were lower, with average thicknesses of 82.3 nm and 92.9 nm, respectively. At 43 °C, there was a lack of saturation, and the five produced films had different thicknesses and the lowest average thickness of 47.5 nm. The further increase in temperature to 67 °C and 74 °C did not result in thickness gain, but rather in a decrease to 99.5 nm and 98.4 nm, respectively, which can be explained by the decomposition of the precursor at higher temperatures, resulting in an overall thickness decrease.

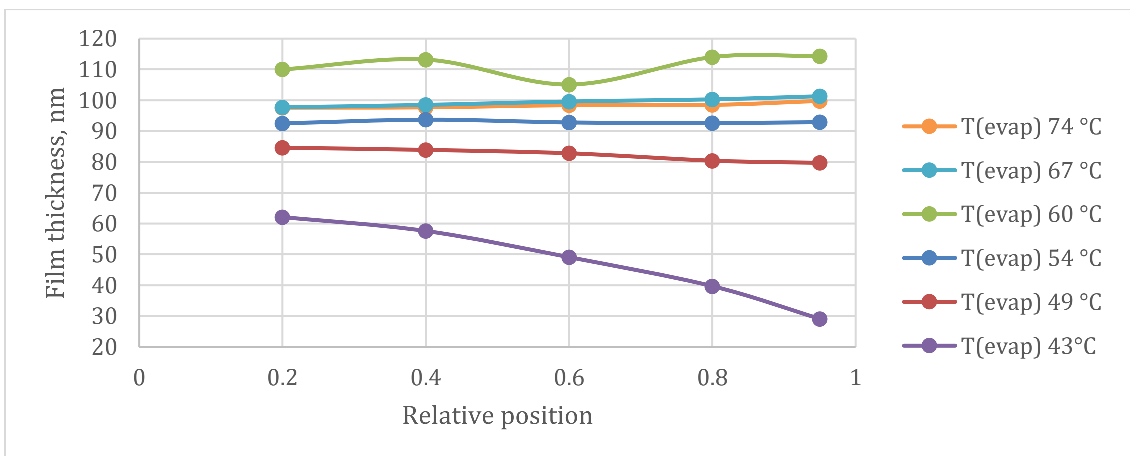

Figure 23. Ellipsometry measurements of Thickness vs T(evap).

5.3 Precursor pulse length influence

5.3.1 Dose of AHEAD

First experiment in this group features change in AHEAD precursor pulse length x, while ozone pulse was unchanged, timing set looks like x/2/5/5 s. The graph in (Figure 24) shows a logical increase in thickness as the AHEAD pulse increases, but after 4 seconds, the increase becomes slight: average thickness 56.6 nm (6s) and 57.3 nm (8s) from original 56.7 nm at 4s. This behaviour may be induced by oversaturation, as excessive overflow of precursor molecules does not contribute significantly to additional growth after the surface has reached its adsorption limit. These results suggest that there is no need to increase the pulse length after six seconds, and it will only increase the overall deposition time. Depositing with a time set of 2/2/5/5 seconds still results in a reasonable average thickness of about 52.4 nm and reduces the time consumption of the ALD process.

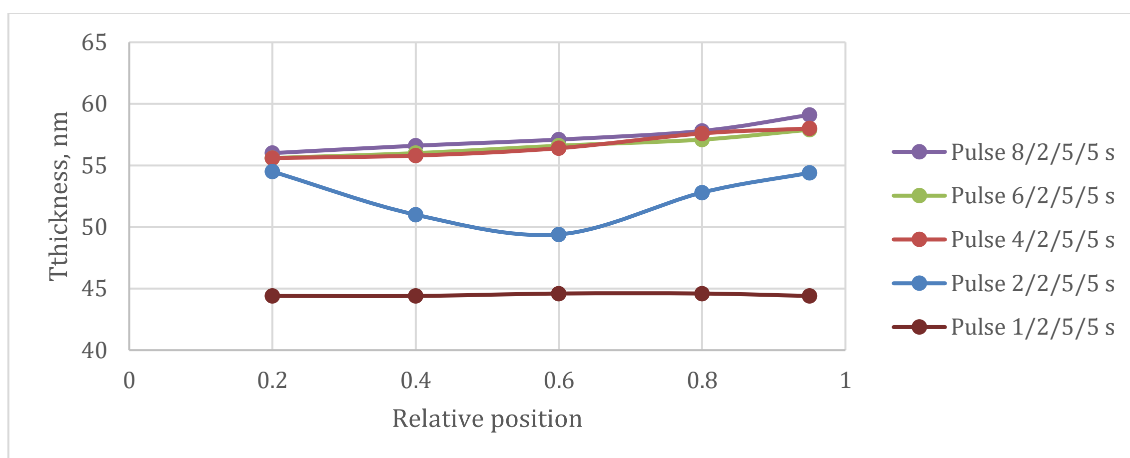

Figure 24. Ellipsometry measurements results of Thickness vs AHEAD pulse.

5.3.2 Dose of ozone

The second deposition series were related to a change in the ozone precursor pulse length. The AHEAD pulse remains unchanged, with a parameter set of 2/2/x/5 seconds, with “x” to be ozone pulse. The impact of pulse change looks at some point similar to AHEAD precursor tendency, with increase in ozone pulse length the thickness will increase too, but without limit point. On Figure 25 an increase in average thickness can be seen: 42.9 (2s) $<$ 45.1 (3s) $<$ 46.7 (4s) $<$ 52.4 (5s) $<$ 53.6 (10s) $<$ 57.5 (15s) nm. It can be suggested that there is a threshold point, below which the increase in thickness is relatively gradual,

but above it the rate of increase becomes more significant. The decision to double the ozone pulse time from 5 seconds to 10 seconds was made to introduce a significant and noticeable change in the precursor parameter. This was done in order to facilitate a more focused exploration of its effect on the resulting film thickness during SiO2 thin film deposition. Also, the decision to double the pulse length was accurate, as an increase from the 5-10 second range would probably have been insignificant. At some point, for further increases in thickness beyond the 5 second mark, the pulse rate in the zone would need to be doubled or tripled.

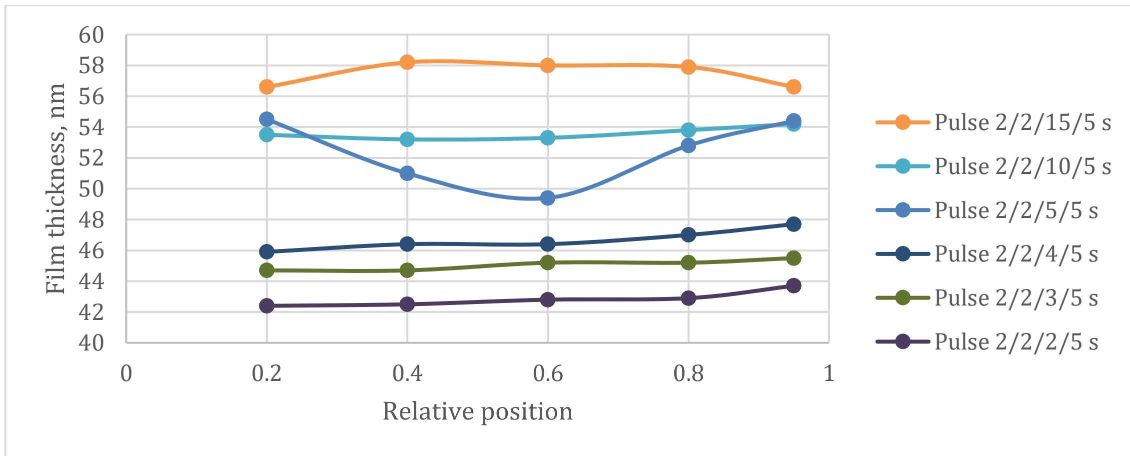

Figure 25. Ellipsometry measurements results of Thickness vs ozone pulse.

5.4 Conclusion

Experiments on the growth temperature in the ALD process revealed two primary findings based on ellipsometry and XRF measurements.

Starting with growth temperature, the gradient analysis indicated that the most uniform samples were produced within the 180-360 °C range (Figure 18), whereas other depositions outside this range failed to reach a Si/O ratio of 0.5. However, even within the optimal range, the Si/O ratio varied significantly: 0.541 at 180 °C, 0.419 at 240 °C, 0.571 at 300 °C, and 0.534 at 360 °C. The low ratio at 240 °C could be attributed to either measurement error or a failed deposition, while 480 °C may be too high for this particular precursor.

Ellipsometry results, on the other hand, showed that the highest average thickness was achieved at 120 °C (118.3 nm) and 180 °C (119 nm), while the most uniform samples were found to be at 300 °C (Figure 22).

Experiments with precursor evaporation temperature for hexakis(ethylamino)disilane revealed that 60 °C is optimal for producing thicker films, achieving an average thickness of 111.3 nm if we compare it to other temperatures. However, at 67 and 74 °C, the films exhibited greater thickness uniformity across five samples, with a more favourable Si/O ratio of 0.499 and 0.486, compared to 0.419 at 60 °C. Therefore, two temperature set points are recommended: 60 °C for applications prioritizing thickness, and 67 or 74 °C for applications requiring a higher Si/O ratio.

The investigation into the impact of precursor pulse lengths showed that set points of 4/2/5/5 seconds, 6/2/5/5, and 8/2/5/5 yielded the highest thicknesses Figure 24, with a general increase in thickness from the first to the last sample, resulting in a ~3 nm difference. The 1/2/2/5 second sample has the best uniformity, with all samples having thicknesses within the range of 44.4 to 44.6 nanometres, but it can be seen from Table 6 that this set point has a Si/O ratio of 0.649 that can't be considered good if we need it to be 0.5. The 2/2/5/5, 4/2/5/5 samples have the lowest ratios of 0.460 and 0.434, respectively, while the 6/2/5/5 and 8/2/5/5 have ratios of 0.559 and 0.518. This suggests that the Si/O ratio approaches 0.5 as the AHEAD precursor introduction time increases. At the same time, the chemical composition graph shows that there is non-uniformity in the deposition across the samples (Figure 20).

The final parameter investigated was the ozone pulse length. Ellipsometry measurements indicate that better uniformity can be achieved at 2/2/2/5 seconds, 2/2/3/5 seconds, and 2/2/4/5 seconds, with higher average thicknesses of 57.5 nm at 2/2/15/5 seconds (Figure 25). This requires tripling the ozone pulse compared to the original 2/2/5/5 second pulse. Regarding the Si/O ratios of the deposited films, in most cases, the ratio of 0.5 has been exceeded (Table 6). The closest value is achieved at 2/2/2/5 seconds (0.499), and the lowest is at 2/2/5/5 seconds (0.460). At the same time, the chemical composition graph indicates that all samples exhibit non-uniformity, which is depicted as waves (Figure 21).

Considering all the data collected, some assumptions about experiments can be made. One of the main problems is rather strange XRF results for deposition series, especially for precursor pulse length and purge time. In most cases, graphs show wave-like shapes rather than straight lines, which indicates non-uniformity.

One possible explanation for these results is that there may be errors in the measurement of Mo samples, or some samples could have been damaged during exploitation, as it was assumed with deposition at a growth temperature of 240 °C.

The second assumption is issues with the Mo samples. The Mo samples may be larger than 10 mm to obtain more accurate scan results, so the data in this way could be collected better.

The third possibility is that the gradient and chemical composition may not accurately reflect the true picture of the ALD window for this precursor. Although ellipsometry may introduce minor errors, overall trends in thickness and uniformity still support the validity of the ALD window. This way, one of the explanations may be hidden in the precursor chemical class. By being one of the aminosilanes, it is quite possible that at certain temperature ranges, precursor behaviour might result in undesirable results. This way, 90 °C results in poor reactivity of the precursor, and temperatures above 360°C mostly result in a risk of decomposition, non-uniformity, and defects.

The fourth option may lie in the selected timing of 2/2/5/5 s for all temperature effect measurements. It is quite possible that at this timing may be problems with deposition reaction, which may result in non-uniformity of produced films. This idea is supported mostly by ratio measurements and studies of precursor pulse effect, where the timing of 2/2/5/5 s, where the ratio of Si/O2 was lower than 0.5, and the produced film thickness was non-uniform across 5 subjects. On the other hand, an increase in precursor introduction times resulted in somewhat closer to uniform films with better ratio, as an example, timing of 8/2/5/5 s with ratio of 0.518 and 2/2/10/5 s with ratio of 0.527. It can also be noticed that a further increase in ozone pulse does not result in a film thickness limit as time rises.

Nonetheless, some anomalies should be considered. During the early deposition series based on growth temperature, a potential leak in the ALD reactor was suspected by the supervisor. The potentially faulty part was replaced, but this issue may have influenced the results of those series. However, even the data from uniformity and ALD window behaviour, with the possibly faulty reactor, still showed general trends of repeated depositions differing mainly in thickness, so it can still be utilized, but it wasn't used in this work. More details regarding the leak are provided in the appendix [7.4].

Overall, it can be considered that possible ALD window range for AHEAD precursors are 180-360 °C for reaction temperature and 60-67 °C range for precursor evaporation. Regarding pulse length recommended avoidance of 2/2/5/5 s timing, or at least doubling of precursors introduction times.

6 SUMMARY

This thesis explored the deposition of SiO_2 thin films using atomic layer deposition (ALD) with hexakis(ethylamino)disilane (AHEAD) as the silicon precursor and ozone as the oxygen precursor. The research focused on understanding how various process parameters, such as growth temperature, precursor evaporation temperature, pulse and purge duration, affect film thickness, uniformity, and chemical composition, particularly the Si/O ratio.

Temperature of reaction for AHEAD deposition with O3 is assumed to be somewhere between 180-360 °C, where probably lies the ALD window.

Precursor evaporation at 60 °C produced the thickest films, while higher evaporation temperatures, 67 °offered better uniformity and closer-to-ideal Si/O ratios, suggesting a 60-67 °C evaporation range for AHEAD

Adjustments to precursor and ozone pulse lengths demonstrated that longer precursor pulses tend to improve the Si/O ratio, while ozone pulse length influenced both thickness and film uniformity.

Overall, the study confirms that precise tuning of ALD parameters is crucial for achieving desired thin film properties. While some challenges were encountered, the research successfully identified optimal conditions for different film requirements. These insights contribute to a better understanding of the ALD process using the AHEAD precursor and offer practical guidance for future applications in the semiconductor and nanotechnology fields.

References

1. T. Justin Kunene, L. Kwanda Tartibu, K. Ukoba, and T.-C. Jen, 'Review of atomic layer deposition process, application and modeling tools', *Materials Today: Proceedings*, vol. 62, pp. S95–S109, Jan. 2022, doi: 10.1016/j.matpr.2022.02.094.
2. R. L. Puurunen, 'Surface chemistry of atomic layer deposition: A case study for the trimethylaluminum/water process', *Journal of Applied Physics*, vol. 97, no. 12, p. 121301, Jun. 2005, doi: 10.1063/1.1940727.
3. R. W. Johnson, A. Hultqvist, and S. F. Bent, 'A brief review of atomic layer deposition: from fundamentals to applications', *Materials Today*, vol. 17, no. 5, pp. 236–246, Jun. 2014, doi: 10.1016/j.mattod.2014.04.026.
4. M. Pan, 'A comparative study of silicon dioxide thin film deposition techniques and the fabrication of ultra-low refractive index nano-porous silicon dioxide thin film', *Graduate Theses and Dissertations*, Jan. 2008, [Online]. Available: https://ecommons.udayton.edu/graduate_theses/4822
5. P. Vitanov, A. Harizanova, T. Ivanova, and H. Dikov, 'Low-temperature deposition of ultrathin SiO2 films on Si substrates', *J. Phys.: Conf. Ser.*, vol. 514, no. 1, p. 012010, May 2014, doi: 10.1088/1742-6596/514/1/012010.
6. M.F.J. Vos, A.J.M. Mackus, W.M.M. Kessels. Atomic Layer Deposition Process Development – 10 steps to successfully develop, optimize and characterize ALD recipes. **2019**, 3. AtomicLimits. Link
7. S. M. George, 'Atomic Layer Deposition: An Overview', *Chem. Rev.*, vol. 110, no. 1, pp. 111–131, Jan. 2010, doi: 10.1021/cr900056b.
8. A. Kurek, P. G. Gordon, S. Karle, A. Devi, and S. T. Barry, 'Recent Advances Using Guanidinate Ligands for Chemical Vapour Deposition (CVD) and Atomic Layer Deposition (ALD) Applications', *Aust. J. Chem.*, vol. 67, no. 7, pp. 989–996, Jun. 2014, doi: 10.1071/CH14172.
9. E. Riyanto *et al.*, 'A review of atomic layer deposition for high lithium-ion battery performance', *Journal of Materials Research and Technology*, vol. 15, pp. 5466–5481, Nov. 2021, doi: 10.1016/j.jmrt.2021.10.138.
10. B. A. Sperling, B. Kalanyan, and J. E. Maslar, 'Atomic Layer Deposition of Al2O3 Using Trimethylaluminum and H2O: The Kinetics of the H2O Half-Cycle', *J. Phys. Chem. C*, vol. 124, no. 5, pp. 3410–3420, Feb. 2020, doi: 10.1021/acs.jpcc.9b11291.
11. P. Boryło *et al.*, 'Structure and properties of Al2O3 thin films deposited by ALD process', *Vacuum*, vol. 131, pp. 319–326, Sep. 2016, doi: 10.1016/j.vacuum.2016.07.013.
12. F. Zahoor *et al.*, 'Resistive random access memory: introduction to device mechanism, materials and application to neuromorphic computing', *Discover Nano*, vol. 18, no. 1, p. 36, Mar. 2023, doi: 10.1186/s11671-023-03775-y.
13. M. Gutsche, H. Seidl, T. Hecht, S. Kudelka, and U. Schroeder, 'Atomic Layer Deposition for advanced DRAM applications', *Future Fab International*, vol. 15, Jan. 2003.
14. S. W. Ryu, J.-G. Song, H. G. Kim, H. Kim, and H.-B.-R. Lee, 'Interlayer-assisted atomic layer deposition of MgO as a magnetic tunneling junction insulators', *Journal of Alloys and Compounds*, vol. 747, pp. 505–510, May 2018, doi: 10.1016/j.jallcom.2018.03.021.
15. Z. Yan *et al.*, 'Atomic layer deposition technology for the development of high-quality, full-colour micro-LED displays', *Next Nanotechnology*, vol. 5, p. 100051, Jan. 2024, doi: 10.1016/j.nxnano.2024.100051.
16. Md. A. Hossain *et al.*, 'Atomic layer deposition enabling higher efficiency solar cells: A review', *Nano Materials Science*, vol. 2, no. 3, pp. 204–226, Sep. 2020, doi: 10.1016/j.nanoms.2019.10.001.
17. K. Erwin, K. Harm, W. Matthieu, M. Adrie, and C. Mariadriana, 'Atomic Layer Deposition of Nanomaterials for Li-Ion Batteries, Fuel Cells, and Solar Cells'. Accessed: May 17, 2024. [Online]. Available: https://www.sigmaaldrich.com/EE/en/technical-documents/technical-article/materials-science-and-engineering/batteries-supercapacitors-and-fuel-cells/atomic-layer-deposition-of-nanomaterials-for-li-ion-batteries-fu
18. T. O. Kääriäinen, P. Maydannik, D. C. Cameron, K. Lahtinen, P. Johansson, and J. Kuusipalo, 'Atomic layer deposition on polymer based flexible packaging materials: Growth characteristics and diffusion barrier properties', *Thin Solid Films*, vol. 519, no. 10, pp. 3146–3154, Mar. 2011, doi: 10.1016/j.tsf.2010.12.171.

19. S. Y. Lee, J. Mack, H. Young Kim, S.-H. Jung, S. J. Rathi, and N. Mukherjee, 'Diffusion barrier properties of atomic layer deposited TiSiN films', *Materials Letters*, vol. 315, p. 131912, May 2022, doi: 10.1016/j.matlet.2022.131912.
20. I. M. Abdulagatov, A. M. Maksumova, M. Z. Magomedov, R. O. Tsakhaeva, S. M. Khidirova, and A. M. Salikhov, 'Antibacterial Food Packaging Nanomaterial Based on Atomic Layer Deposition for Long-Term Food Storage', *J Food Sci Technol*, vol. 61, no. 3, pp. 596–606, Mar. 2024, doi: 10.1007/s13197-023-05867-0.
21. *Novel nanostructured polymeric materials for food packaging and beyond: Novel nanostructured polymeric materials for foodpackaging and beyond*. in VTT Symposium. VTT Technical Research Centre of Finland, 2011.
22. R. S. Pessoa and M. A. Fraga, 'Chapter 11 - Biomedical applications of ultrathin atomic layer deposited metal oxide films on polymeric materials', in *Frontiers of Nanoscience*, vol. 14, M. Benelmekki and A. Erbe, Eds., in Nanostructured Thin Films, vol. 14. , Elsevier, 2019, pp. 291–307. doi: 10.1016/B978-0-08-102572-7.00011-8.
23. M. Shahmohammadi, B. Yang, and C. G. Takoudis, 'Applications of Titania Atomic Layer Deposition in the Biomedical Field and Recent Updates', *AJBSR*, vol. 8, no. 5, p. 465, May 2020.
24. E. Acosta, 'Thin Films/Properties and Applications', in *Thin Films*, IntechOpen, 2021. doi: 10.5772/intechopen.95527.
25. V. S. K. Channam, 'Synthesis of strongly correlated oxides and investigation of their electrical and optical properties', 2017. link
26. H.-J. Freund, 'Clusters and islands on oxides: from catalysis via electronics and magnetism to optics', *Surface Science*, vol. 500, no. 1, pp. 271–299, Mar. 2002, doi: 10.1016/S0039-6028(01)01543-6.
27. K. A. Lozovoy, A. G. Korotaev, A. P. Kokhanenko, V. V. Dirko, and A. V. Voitsekhovskii, 'Kinetics of epitaxial formation of nanostructures by Frank–van der Merwe, Volmer–Weber and Stranski–Krastanow growth modes', *Surface and Coatings Technology*, vol. 384, p. 125289, Feb. 2020, doi: 10.1016/j.surfcoat.2019.125289.
28. T. Hatanpää, M. Ritala, and M. Leskelä, 'Precursors as enablers of ALD technology: Contributions from University of Helsinki', *Coordination Chemistry Reviews*, vol. 257, no. 23, pp. 3297–3322, Dec. 2013, doi: 10.1016/j.ccr.2013.07.002.
29. G. S. Oehrlein, D. Metzler, and C. Li, 'Atomic Layer Etching at the Tipping Point: An Overview', *ECS J. Solid State Sci. Technol.*, vol. 4, no. 6, p. N5041, Mar. 2015, doi: 10.1149/2.0061506jss.
30. P. Vajeeston, H. Fjellvåg, and O. Nilsen, 'Search for potential precursors for Si-atomic layer deposition – A quantum chemical study', *Materials Letters*, vol. 216, pp. 189–192, Apr. 2018, doi: 10.1016/j.matlet.2018.01.040.
31. V. Y. Vasilyev, 'Review—Atomic Layer Deposition of Silicon Dioxide Thin Films', *ECS J. Solid State Sci. Technol.*, vol. 10, no. 5, p. 053004, May 2021, doi: 10.1149/2162-8777/abffab.
32. 'Silane', *Wikipedia*. May 02, 2024. Accessed: May 17, 2024. [Online]. Available: https://en.wikipedia.org/w/index.php?title=Silane&oldid=1221820708
33. 'Chemical Vapor Deposition of Three Aminosilanes on Silicon Dioxide: Surface Characterization, Stability, Effects of Silane Concentration, and Cyanine Dye Adsorption | Langmuir'. Accessed: May 17, 2024. [Online]. Available: https://pubs.acs.org/doi/10.1021/la102447y
34. B. Johnson, C. Cushman, B. Lunt, M. Kaykhaii, and M. Linford, 'An Introduction to Silanes, their Chemical Vapor Deposition onto Si/SiO2, and Characterization of the Resulting Monolayers', *Vacuum Technology & Coating*, Jun. 2016, [Online]. Available: https://www.researchgate.net/publication/303486340_An_Introduction_to_Silanes_their_Chemical_Vapor_Deposition_onto_SiSiO2_and_Characterization_of_the_Resulting_Monolayers
35. N. Hong *et al.*, 'The Evolution of Organosilicon Precursors for Low-k Interlayer Dielectric Fabrication Driven by Integration Challenges', *Materials*, vol. 14, no. 17, Art. no. 17, Jan. 2021, doi: 10.3390/ma14174827.
36. K. Raudonen, 'SYNTHESIS, ANALYSIS, AND APPLICATION OF GRAPHENE LAYERS FOR FUNCTIONAL DEVICES', [Online]. Available: https://dspace.ut.ee/server/api/core/bitstreams/b8f086fc-63c1-4f3f-9044-1f1526a82ecd/content
37. T. Kahro *et al.*, 'Nanostructures Stacked on Hafnium Oxide Films Interfacing Graphene and Silicon Oxide Layers as Resistive Switching Media', *Nanomaterials*, vol. 13, no. 8, Art. no. 8, Jan. 2023, doi: 10.3390/nano13081323.
38. J. Cho, T. Kim, T. Seegmiller, and J. P. Chang, 'Mechanistic study of atomic layer deposition of AlxSiyO thin film via in-situ FTIR spectroscopy', *Journal of Vacuum Science & Technology A*, vol. 33, no. 5, p. 05E130, Aug. 2015, doi: 10.1116/1.4927318.

39. K. Kukli *et al.*, 'Magnetic properties and resistive switching in mixture films and nanolaminates consisting of iron and silicon oxides grown by atomic layer deposition', *Journal of Vacuum Science & Technology A*, vol. 38, no. 4, p. 042405, Jun. 2020, doi: 10.1116/6.0000212.
40. Y. Tomczak *et al.*, 'In Situ Reaction Mechanism Studies on Atomic Layer Deposition of AlxSiyOz from Trimethylaluminium, Hexakis(ethylamino)disilane, and Water', *Chem. Mater.*, vol. 24, no. 20, pp. 3859–3867, Oct. 2012, doi: 10.1021/cm301658m.
41. K. Kukli *et al.*, 'Silicon oxide-niobium oxide mixture films and nanolaminates grown by atomic layer deposition from niobium pentaethoxide and hexakis(ethylamino) disilane', *Nanotechnology*, vol. 31, no. 19, p. 195713, Feb. 2020, doi: 10.1088/1361-6528/ab6fd6.
42. 'What is Spectroscopic Ellipsometry?', AZoM. Accessed: May 17, 2024. [Online]. Available: https://www.azom.com/article.aspx?ArticleID=17486
43. 'High-Speed Spectroscopic Ellipsometer Principle and Structure｜Fundamentals of High-Speed Spectroscopic Ellipsometer｜How to｜ULVAC SHOWCASE', ULVAC SHOWCASE. Accessed: May 17, 2024. [Online]. Available: https://showcase.ulvac.co.jp/en/how-to/product-knowledge08/principle.html
44. 'Technology Information', Multi-Wavelength Ellipsometers - Film Sense. Accessed: May 17, 2024. [Online]. Available: https://film-sense.com/ellipsometry-technology/
45. F. L. McCrackin, E. Passaglia, R. R. Stromberg, and H. L. Steinberg, 'Measurement of the thickness and refractive index of very thin films and the optical properties of surfaces by ellipsometry', *J. RES. NATL. BUR. STAN. SECT. A.*, vol. 67A, no. 4, p. 363, Jul. 1963, doi: 10.6028/jres.067A.040.
46. Ellipsometry review document provided by Aarne Kasikov, Institute of Physics, University of Tartu, aarnek@ut.ee
47. 'What is X-ray Fluorescence (XRF)'. Accessed: May 17, 2024. [Online]. Available: https://www.horiba.com/int/scientific/technologies/energy-dispersive-x-ray-fluorescence-ed-xrf/what-is-x-ray-fluorescence-xrf/
48. H. H.-T. Corporation, 'Principle of XRF Analysis', Hitachi High-Tech Corporation. Accessed: May 17, 2024. [Online]. Available: https://www.hitachi-hightech.com/global/en/knowledge/analytical-systems/xrf/xrf-descriptions.html
49. K. Sharma, 'X-ray Fluorescence Spectrometry: Principle, Instrumentation, and Application'. Accessed: May 17, 2024. [Online]. Available: https://scienceinfo.com/x-ray-fluorescence-spectrometry-principle/
50. A. Vermeer, F. Roozeboom, P. Poodt, and R. Gortzen, 'High Throughput, Low Cost Deposition of Alumina Passivation Layers by Spatial Atomic Layer Deposition', *MRS Proceedings*, vol. 1323, Jan. 2011, doi: 10.1557/opl.2011.959.
51. D. Muñoz-Rojas, V. H. Nguyen, C. M. de la Huerta, S. Aghazadehchors, C. Jiménez, and D. Bellet, 'Spatial Atomic Layer Deposition (SALD), an emerging tool for energy materials. Application to new-generation photovoltaic devices and transparent conductive materials', *Comptes Rendus. Physique*, vol. 18, no. 7–8, pp. 391–400, 2017, doi: 10.1016/j.crhy.2017.09.004.
52. 'Area-Selective Deposition: Fundamentals, Applications, and Future Outlook | Chemistry of Materials'. Accessed: May 17, 2024. [Online]. Available: https://pubs.acs.org/doi/10.1021/acs.chemmater.0c00722
53. K. K. Mentel, A. V. Emelianov, A. Philip, A. Johansson, M. Karppinen, and M. Pettersson, 'Area-Selective Atomic Layer Deposition on Functionalized Graphene Prepared by Reversible Laser Oxidation', *Advanced Materials Interfaces*, vol. 9, no. 29, p. 2201110, 2022, doi: 10.1002/admi.202201110.
54. A. J. M. Mackus, M. J. M. Merkx, and W. M. M. Kessels, 'From the Bottom-Up: Toward Area-Selective Atomic Layer Deposition with High Selectivity', *Chem. Mater.*, vol. 31, no. 1, pp. 2–12, Jan. 2019, doi: 10.1021/acs.chemmater.8b03454.
55. 'Area-Selective Deposition: Fundamentals, Applications, and Future Outlook | Chemistry of Materials'. Accessed: May 17, 2024. [Online]. Available: https://pubs.acs.org/doi/10.1021/acs.chemmater.0c00722
56. V. Miikkulainen, K. Väyrynen, K. Mizohata, J. Räisänen, M. Vehkamäki, and M. Ritala, 'Photoassisted atomic layer deposition of oxides employing alkoxides as single-source precursors', *Journal of Vacuum Science & Technology A*, vol. 37, no. 6, p. 060911, Nov. 2019, doi: 10.1116/1.5124100.
57. V. Miikkulainen *et al.*, '(Invited) Photo-Assisted ALD: Process Development and Application Perspectives', *ECS Trans.*, vol. 80, no. 3, p. 49, Aug. 2017, doi: 10.1149/08003.0049ecst.

58. E. A. Irene, ‘SiO2 Based MOSFETS: Film Growth and Si—SiO2 Interface Properties’, in *High Dielectric Constant Materials: VLSI MOSFET Applications*, H. R. Huff and D. C. Gilmer, Eds., Berlin, Heidelberg: Springer, 2005, pp. 45–90. doi: 10.1007/3-540-26462-0_3.
59. K. Pfeiffer *et al.*, ‘Comparative study of ALD SiO_2 thin films for optical applications’, *Opt. Mater. Express, OME*, vol. 6, no. 2, pp. 660–670, Feb. 2016, doi: 10.1364/OME.6.000660.
60. N. Tajima, H. Murotani, and T. Matsudaira, ‘Optical multicoating using low-refractive-index SiO2 optical thin films deposited by sputtering and electron beam evaporation’, *Thin Solid Films*, vol. 776, p. 139824, Jul. 2023, doi: 10.1016/j.tsf.2023.139824.
61. X. He, J. Wu, L. Wu, L. Zhao, X. Gao, and X. Li, ‘Structure, morphology and optical properties of SiO2−x thin films prepared by plasma-assisted pulsed laser deposition’, *Applied Surface Science*, vol. 254, no. 6, pp. 1730–1735, Jan. 2008, doi: 10.1016/j.apsusc.2007.07.127.
62. ‘Optical Coatings’, Shanghai Optics. Accessed: May 17, 2024. [Online]. Available: https://www.shanghai-optics.com/about-us/resources/technical-articles/types-of-optical-coatings/
63. ‘Optical thin films ｜ Products ｜ AGC’. Accessed: May 17, 2024. [Online]. Available:https://www.agc.com/en/products/electoric/optical_coating/top.html#:~:text=An%20optical%20thin%20film%20is,designing%20the%20thickness%2C%20material%2C%20and

7 Appendix

7.1 Reactor description and set up

Before initiation of any ALD deposition, it is important to check availability and compatibility of precursors, gases and other co-reactants which are utilized in deposition process. Also, it is recommended to check capability of reactor to perfume desired deposition of choice.

In our case, the thermal ALD reactor was used in all deposition experiments made in this research work. All process were adjusted and manipulated from computer, to which as well all the measurement devices were connected (Figure 26).

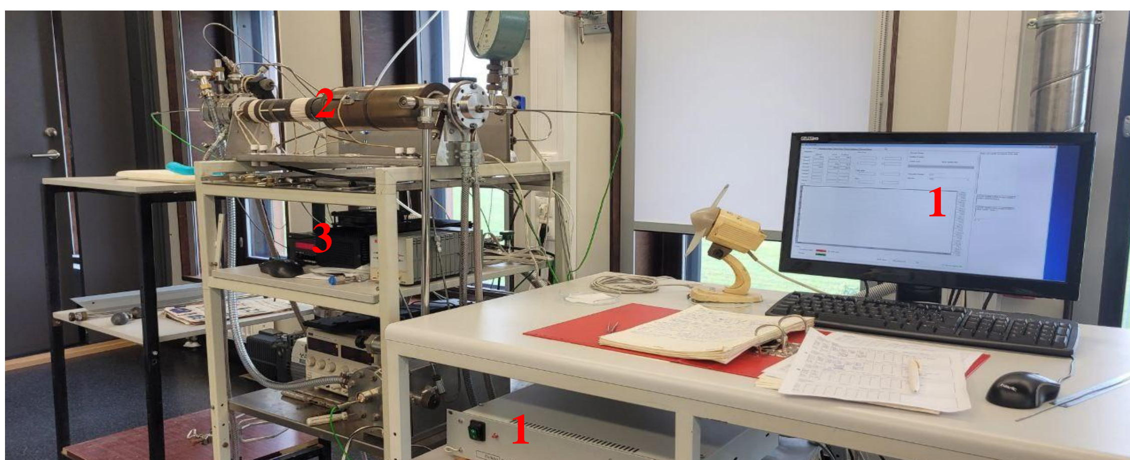

Figure 26. Working place: 1 - Computer and measurement devices connected to it, 2 - ALD reactor, 3 - Ozone generator and measurement device

On Figure 27 we can see the other main part of reactor the nitrogen induction lines. When, inert gas is introduced to fill the reactor it excludes oxygen entering it and preventing any reactions inside, maintaining reactor inert atmosphere and clean it if needed (Figure 27).

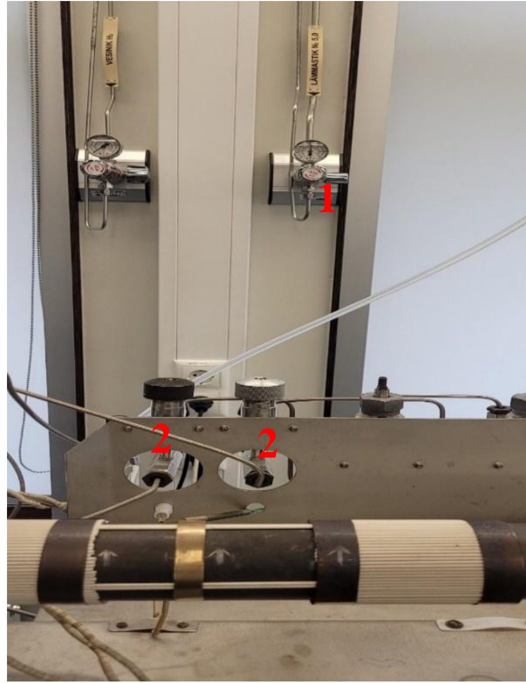

Figure 27. Nitrogen introduction: 1 - Nitrogen line, 2 - Nitrogen entrance to ALD reactor

Other part of the reactor is growth chamber, where deposition process occurs. The substrate holder was put to growth chamber and closed with flange which has a hole for thermocouple insertion (Figure 28) (Figure 32). Before closing the growth chamber, a spring was inserted beforehand (Figure 29), for ensuring proper sealing and uniform pressure minimizing the risk of uneven sealing or leaks. Also, spring may help to accommodate any thermal expansion or contraction of the reactor components, ensuring that the seal remains intact even under varying temperature conditions.

Figure 28. Samples insertion to ALD reactor, growth chamber

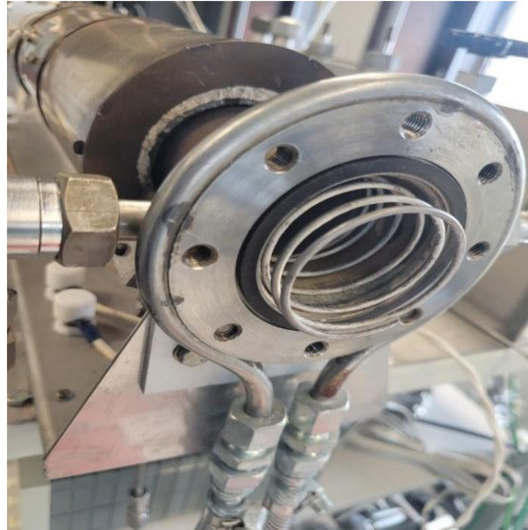

Figure 29: Spring inserted in ALD reactor after sample insertion.

The precursor was introduced into the evaporation chamber with thermocouple on the other side of ALD reactor where evaporation chamber is located (Figure 30) (Figure 32). The precursor in liquid state was placed in tube for containment, with tube featuring hole for possible evaporation (Figure 31). After completion of these manipulation the ALD reactor can be considered as fully assembled (Figure 32).

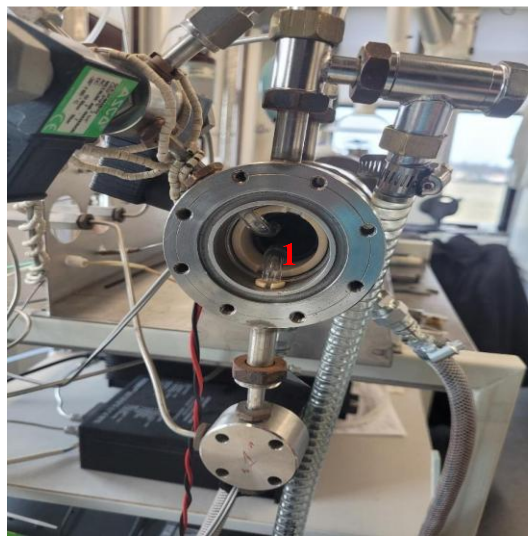

Figure 30. Precursor (AHEAD)insertion to ALD reactor, evaporation chamber. 1 – precursor tube.

Figure 31. Tube for precursor containment inside of evaporation chamber in ALD reactor.

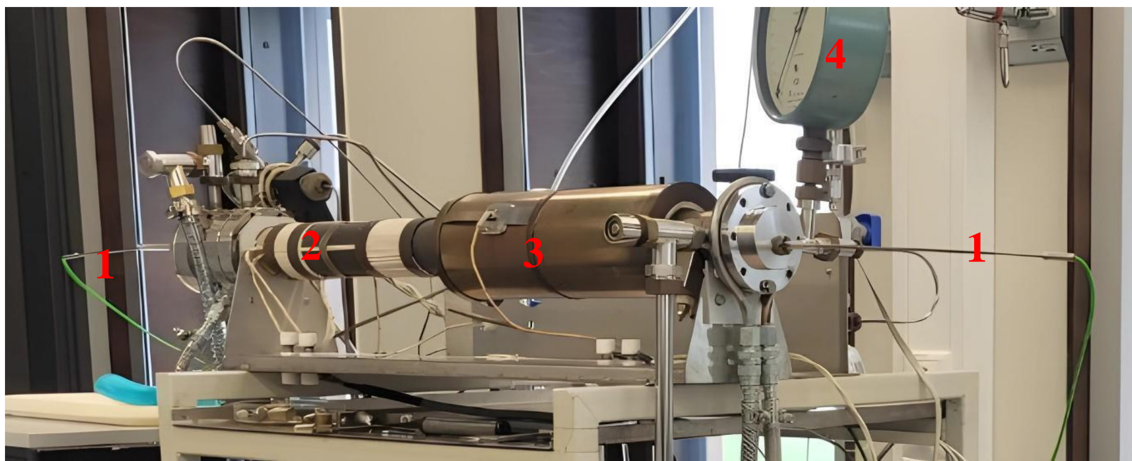

Figure 32. Fully assembled ALD reactor: 1 – Thermocoples, 2 – Evaporation chamber, 3 – Growth chamber, 4 – Pressuremeter.

The next step is to switch on vacuum pump and open the main wall on vacuum generator (Figure 33). The vacuum pump creates a pressure differential between the inside of the pump and the ALD reactor. When the first wall on the pump is opened (Figure 33) (2), it allows the pump to start evacuating the air from its internal chamber. This initiates the process of reducing the pressure inside the pump.

Once the pressure inside the pump has been sufficiently reduced and stabilized, the second wall (Figure 33) (3) is then slowly opened on the ALD reactor. This allows the vacuum from the pump to gradually draw out the nitrogen or other gases from the reactor, controlling the rate of depressurization and ensuring that the process occurs smoothly without sudden pressure surges or fluctuations. If the second wall on the ALD reactor is opened immediately, it could lead to a rapid influx of gas from the reactor into the pump,

causing sudden pressure changes and potential instability in the system, as well as may result in displacement of substrate samples inside growth chamber.

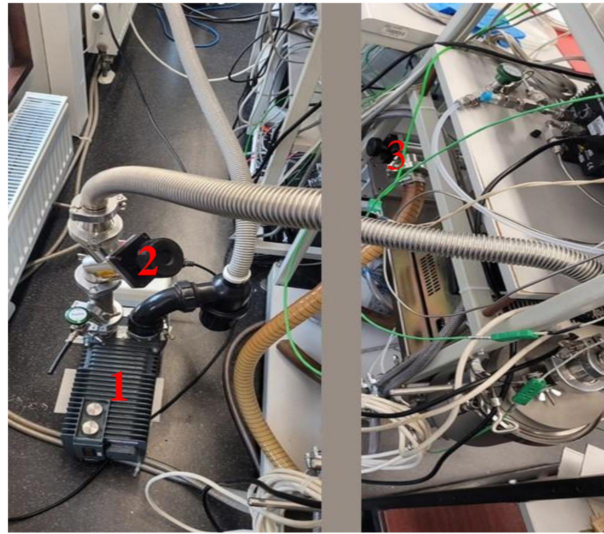

Figure 33. Location of vacuum machine. 1 – Vacuum pump, 2 – First vacuum wall, 3 – Second vacuum wall.

Once pressure stabilized and checked, the oxygen channel can be opened, ozone generator and ozone analyzer powered on (Figure 34), (Figure 35) and (Figure 36). Underneath ozone devices afterburner is located (Figure 37). ALD processes often involve the use of precursor gases and by-products that may be flammable or pose other safety risks. The afterburner provides a means to safely combust any unreacted or harmful gases, reducing the risk of hazardous build-up or release of these gases into the surrounding environment.

Finally, the deposition process can be adjusted on computer, parameters like: purge time, precursor introduction time, temperatures (afterburner, growth and evaporation chambers) and cycle number can be set up. After that, the reactor's heating system turned on. Heating time and ozone generation require approximately one hour before deposition can be initiated.

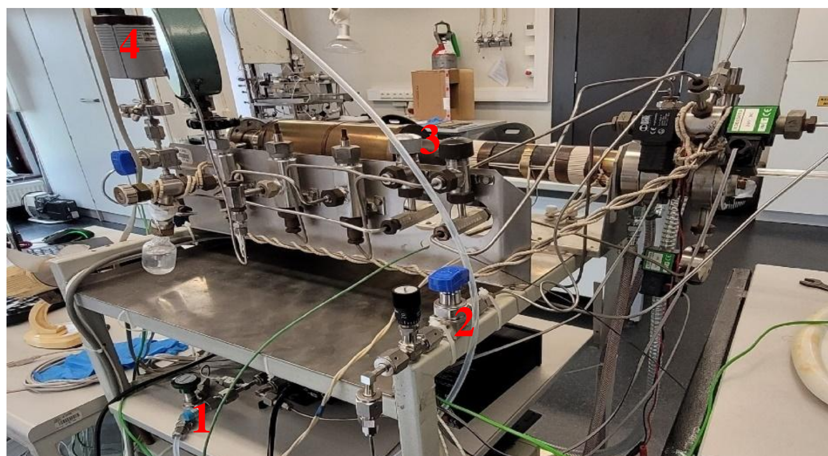

Figure 34. Back view on ALD reactor: 1 – Oxygen line directed to ozone generator, 2 – Ozone line to ALD reactor, 3 – Nitrogen line to ALD reactor, 4 – Wall to open line for pressure measurement device.

Figure 35. Back view on Ozone generator (1) and analyzer (2).

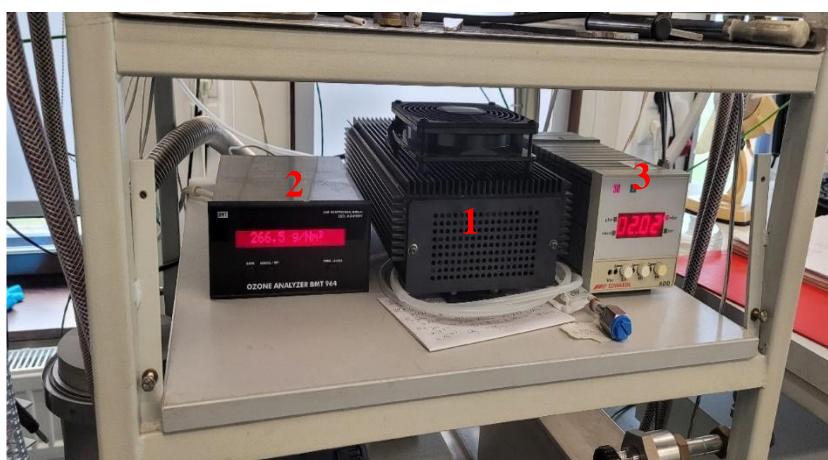

Figure 36. Front view on Ozone generator (1) and analyzer (2), 3 – pressure measurement device.

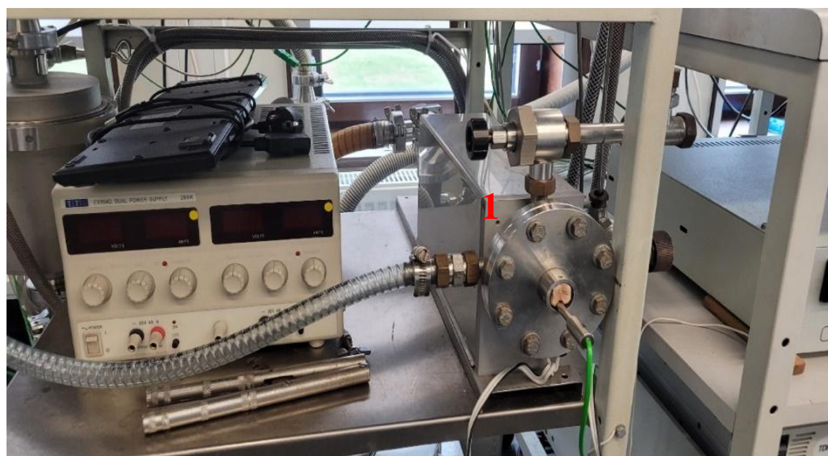

Figure 37. View on afterburner (1).

Upon completion of deposition, the oxygen channel, ozone generator, and ozone analyzer, as well as temperature control can be deactivated or closed (Figure 34), (Figure 35). Cooling of reactor take some time depending on temperature, so addition cooling outside of reactor like cooler can be added to cool off growth chamber.

When cooling is finished the pressure must be returned to state before second wall of vacuum pump was opened, this is made by closing second wall of the pump (Figure 38). Rapid changes in pressure within the reactor can lead to mechanical stress on the reactor components or sudden release of gases, posing safety hazards to personnel and equipment. Abrupt changes in pressure can also affect the integrity of the materials inside the reactor, particularly thin films or delicate substrates. By returning the pressure to its initial state gradually, the risk of accidents, equipment or thin film damage is minimized. After stabilization samples can be taken out and reactor sealed, and filled with nitrogen again, vacuum pump turned off and pressure returned to normal again. All sources then are closed, and devices are powered off.

7.2 Variations of ALD techniques

7.2.1 Spatial ALD

Spatial ALD is based on separation of precursors in space rather than in time, by continuous substrate movement between two rooms filled with a precursor gas. This way the sequential exposures are replicated and purge steps are excluded, reactions take place faster and reactions can be performed at atmospheric pressure. S-ALD (spatial ALD) is easier and less expensive to scale up compared to conventional ALD. However, it may

be sensitive to ambient oxygen and water during processing in air. Additionally, not all precursors can meet the requirements of high volatility [50-51].

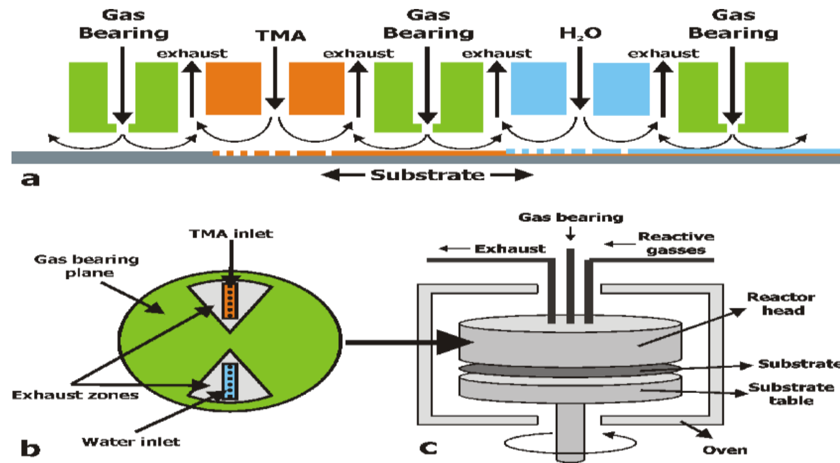

Figure 39. Representation of spatial ALD technique approach. (Adopted from [50])

Spatial ALD reactor differs from most other ALD reactors by change in interaction between precursor and substrate folder. Figure 39, part "a" represents concept of the spatial ALD reactor, where the TMA and water half reaction zones are separated by gas bearings, while underneath the reactor substrate folder is continuously moving. The substrate is exposed to one precursor in one region of the chamber, allowing it to react with the surface and form a monolayer. This separation helps to prevent mixing of the precursors before they reach the substrate. Then, the substrate is moved or the precursor flow is switched, and the substrate is exposed to the second precursor in another region of the chamber. Process is repeated until the desired film thickness is achieved. Figure 39, part "b" gives a view of the bottom side of the spatial ALD reactor head, where the TMA and water half-reaction zones are integrated into inlets surrounded by exhaust zones and gas bearing planes [50]. Figure 39, part "c" is schematic drawing of the reactor. The reactor head and rotating substrate table with the substrate in between are placed in a convection oven. The substrate table is rotated by a servo motor, connected by a drive shaft. The process- and waste gas lines are connected to the reactor head through an opening in the top of the oven [50].

7.2.2 Area selective ALD

Area selective ALD (AS-ALD) technique aims to deposit thin films on specific regions of a substrate while leaving other regions untouched. These techniques aim to manipulate surface chemistries to create local differences, limiting film growth to desired areas. The

most common methods in area selective deposition (ASD) are: intrinsic ASD, surface passivation, surface activation by local energy delivery or catalytic activation (Figure 40).

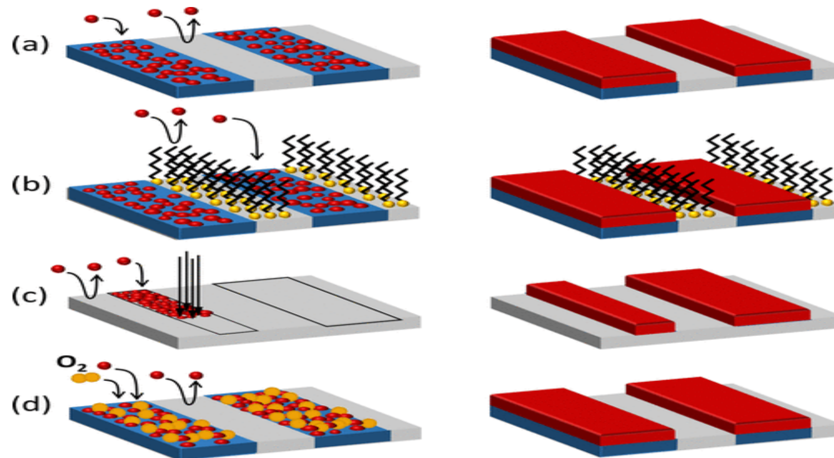

Figure 40. Common approaches for ASD during ALD and CVD: (a) intrinsic ASD; (b) ASD by surface passivation (SAMs); (c and d) surface activation by local energy delivery (panel c) or by local catalytic activation of a reactant (panel d). (Adopted from [52])

Intrinsic or Inherent ASD (Figure 40, part "a") is based on inherent properties of the substrate surface to achieve selective deposition. By precise control of process parameters such as precursor exposure time, temperature, and pulse duration, the differences in surface chemistry can occur, by this way the deposition can be guided to desired regions while avoiding unwanted growth locations. This method is particularly effective when dealing with substrates that naturally exhibit variations in reactivity or surface energy. However, achieving precise control over deposition can be challenging, especially on complex or heterogeneous surfaces. ASD by surface passivation (Figure 40, part "b") involves modifying the substrate surface with a patterned self-assembled monolayer (SAM) to selectively block ALD precursor adsorption in certain regions. SAMs consist of organic molecules with functional end groups that can chemically interact with ALD precursors, inhibiting their adsorption and subsequent film growth or act as barriers to selectively block precursor molecules from specific areas of substrate. Surface activation methods (Figure 40, part "c") involve selectively modifying the substrate surface to enhance ALD precursor adsorption in specific regions [52]. This can be achieved through local energy delivery, such as plasma treatment, laser irradiation, or electron beam activation, which activates surface sites and promotes precursor adsorption. Alternatively, catalytic activation (Figure 40, part "d") involves introducing a catalyst onto the substrate surface, which facilitates surface reactions and enhances precursor adsorption in desired

regions [53-55]. These methods offer precise control over deposition and can be tailored to accommodate a wide range of substrates and deposition conditions. However, achievement of uniformity and scalability across large areas remains a challenge, as variations in surface chemistry and substrate morphology can impact deposition quality. Additionally, the choice of blocking agents or surface modifiers may introduce unintended chemical interactions or surface contamination, necessitating careful optimization and characterization.

7.2.3 Photo-assisted ALD

Photo-assisted atomic layer deposition (PA-ALD), sometimes also called photo-chemical atomic layer deposition (PC-ALD), is a ground-breaking advancement in thin film deposition techniques, implementing light to enhance the deposition process beyond the capabilities of traditional thermal ALD. Light is employed to activate precursor molecules on a substrate surface or within the gas phase. The photons provide energy to break chemical bonds or initiate reactions that would not occur under thermal activation alone. By using light to drive reactions, photo-assisted ALD can enable deposition at lower temperatures and enhance reactivity compared to traditional thermal ALD, similar to plasma-assisted ALD. As compared to plasma-assisted ALD, the activation is weaker, but is often easier to control by adjusting the wavelength, intensity and timing of illumination [56-57]. Moreover PA-ALD can be combined with Area-selective ALD. The principle behind a photo-assisted atomic layer deposition (ALD) reactor involves integrating a photon source, typically ultraviolet (UV) radiation, into a conventional ALD deposition system to enhance or enable specific aspects of the deposition process (Figure 41). The reactor design aims to harness the energy of photons to promote surface reactions, accelerate precursor decomposition, or facilitate the removal of byproducts, thus improving the efficiency, control, and properties of the deposited thin films [56-57].

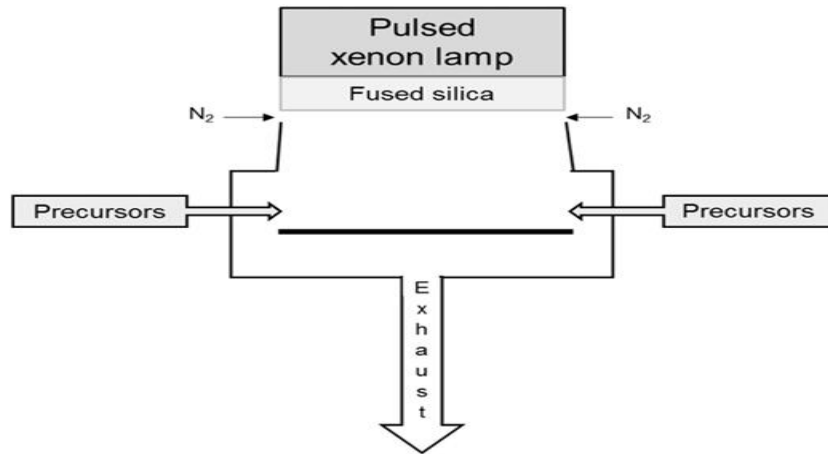

Figure 41. Example of photo-ALD reactor. (Adopted from [56])

While photo-assisted ALD offers several advantages, advantages, such as enhanced deposition rates and improved film control in compare to plasma-assisted ALD, the choice of precursor is limited by precursor photochemical properties and compatibility with the deposition process. The availability of suitable precursors may be limited, posing a challenge for application. Additionally, integrating a light source into the ALD reactor introduces complexity and increases energy consumption, particularly for large-scale production processes. The design and implementation of light sources, optical components, and control systems elevate equipment costs and may require specialized expertise for maintenance and operation. Additionally, high-energy photons used in photo-assisted ALD processes can potentially induce surface damage or introduce defects in sensitive materials, necessitating careful optimization and characterization.

7.3 SiO_2 additions from literature review

7.3.1 SiO_2 in electronics

Silicon dioxide thin films are mostly famous for their electrical properties, particularly their excellent insulation properties, which make them widely used as an insulation layer in modern electronic devices. These good insulation characteristics are due to the high dielectric constant of silicon dioxide, making it a common material for gate dielectrics in semiconductor devices, such as metal-oxide-semiconductor field-effect transistors (MOSFETs) (Figure 42) [58].

MOSFET is a type of semiconductor device that can be used to amplify or switch electronic signals. It consists of three main regions: a source, a drain, and a channel, all

contained within a semiconductor substrate made of silicon [58]. The source and drain are areas where current enters and exits the transistor, respectively. These areas are highly doped regions of the semiconductor material, meaning the concentrations of electron donors and acceptors are high. The channel, which is located between the source and drain, and is usually a thin layer of semiconductor material that can be controlled by an electric field. The gate, typically a metal electrode, which is separated from the channel by a thin insulating layer, which acts as a barrier to prevent current flow between the gate and the channel. This insulating layer is known as the gate dielectric.

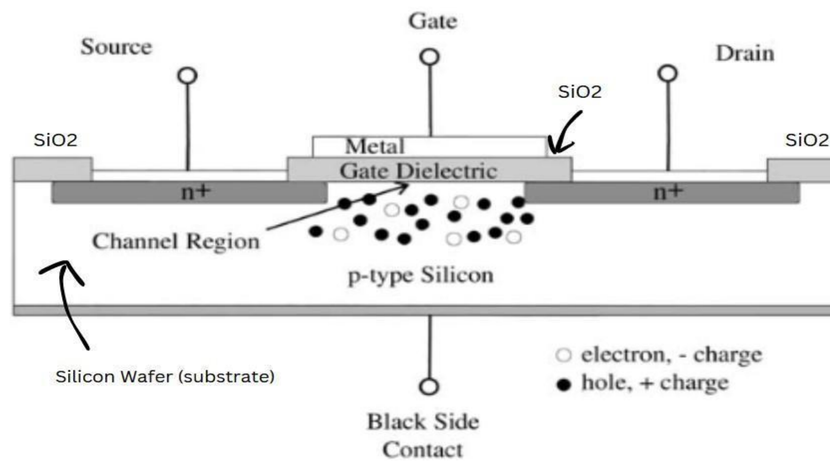

Figure 42. Pictorial representation of an N-Channel MOSFET. The gate dielectric SiO_2 film is located below the metal gate contact and above the channel region of the transistor. (Adopted from [58])

When a voltage is applied across the gate terminal of a MOSFET, it creates an electric field across the insulating layer. If this voltage is above a certain threshold, it attracts or repels carriers (electrons or holes) within the channel. The type of MOSFET determines whether the carriers are attracted or repelled, depending on whether the channel is n-type or p-type. By modulating the gate voltage, the conductivity of the channel can be controlled, allowing the MOSFET to function as a switch or an amplifier. When the gate voltage is lower than a certain threshold value, the channel is depleted of carriers and the device is in the “off” state (high resistance). However, when the gate voltage rises above the threshold, carriers are allowed to flow through the channel and the device becomes conductive, and the MOSFET is in the "on" state (low resistance), allowing current to flow between the source and the drain [58]. The SiO_2 layer acts as the gate insulator in a MOSFET, providing electrical isolation between the gate electrode and the semiconductor channel. This prevents current flow between these two elements, which is essential for the proper functioning of the device. SiO_2 helps to control the threshold

voltage of the MOSFET, reducing leakage current and improving device performance and reliability. Additionally, SiO_2 has excellent dielectric properties, including high breakdown voltage and low defect density. These properties make it suitable for use in MOSFETs operating under high voltages and frequencies, as they ensure the stability and reliability of the devices [58].

7.3.2 SiO_2 in optics

Thin films are commonly used as optical coatings to control the behaviour of light when it interacts with a surface. This includes modifying the amount of light that is transmitted, bent, reflected, or blocked [59-62]. Anti-reflection coatings are designed to minimize reflections and improve visibility, contrast, and clarity at the surface of various optical components. These coatings are used on lenses, windows, displays, and scientific instruments to reduce glare and unwanted reflections, and maximize light transmission (Figure 43) [63].

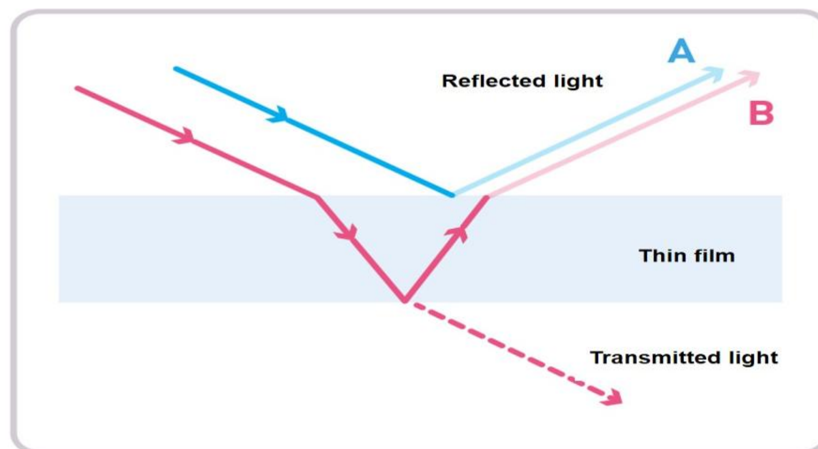

Figure 43. Interaction of light and thin film. (Adopted from [63])

High-reflectivity coatings are used to maximize the amount of light reflected at the surface of optical components such as mirrors and other reflective optics. These coatings increase the reflectance of light over specific wavelength ranges, which allows for efficient light amplification and beam steering in optical systems. They are commonly used in laser systems, telescopes, interferometers; and optical resonators to create high-quality optical cavities and achieve precision measurements [**Error! Reference source not found.**]. On the other hand, low-reflectivity coatings minimize reflections and maintain some level of light transmission of certain wavelengths. These are useful in applications where it is desirable to reduce reflections while still allowing some light to

pass through, such as optical filters, beam splitters, and laser output couplers [62]. Thin films for optical coatings are typically made from a variety of materials chosen for their optical properties, durability, and compatibility with deposition techniques. Common materials used for anti-reflection coatings are dielectrics (SiO_2, TiO_2, HfO_2), fluorides (MgF_2), high-reflective coatings are metals (Al, Ag, Au) and for low-reflectivity are used multi-layered coatings with controlled thickness variations or combinations of dielectric materials such as SiO_2, TiO_2, Ta_2O_5 [59-62]. Achieving minimal absorption and scattering losses is a significant challenge when using dielectric coatings in optical multilayer structures. It is essential to carefully control both the optical thickness and the uniform distribution of film thickness during the preparation process. The surface-controlled growth mechanism provided by atomic layer deposition (ALD) effectively addresses these issues. It allows for remarkable scalability of film thickness at sub-nanometre levels and ensures excellent repeatability without the need for real-time monitoring. By controlling the number of ALD cycles, the resulting film thickness can be precisely modulated. Silicon dioxide (SiO_2) is useful in optics and optical coatings. Not only it can be long-lasting even under high-temperature conditions, but it also has excellent transparency and low refractive index. Silicon oxide has relatively good adhesion with different surfaces and is mechanically resilient [62].

7.4 Anomalies

Some of depositions were performed multiple time at the same temperature and conditions, but resulted thickness was different for each case Table 7 (Figure 44 - Figure 48).

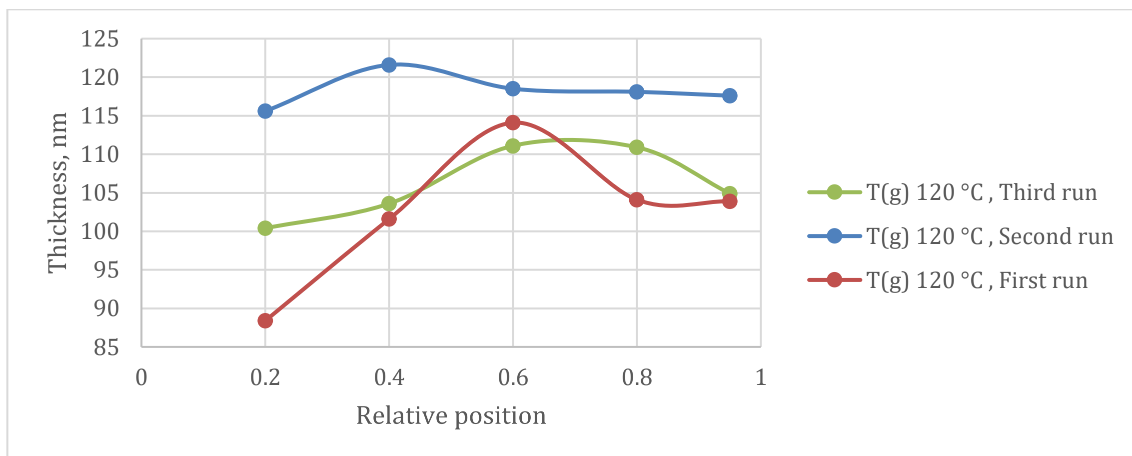

Figure 44: Thickness vs T(g), 1200 cycles, anomalies for 120 C° depositions

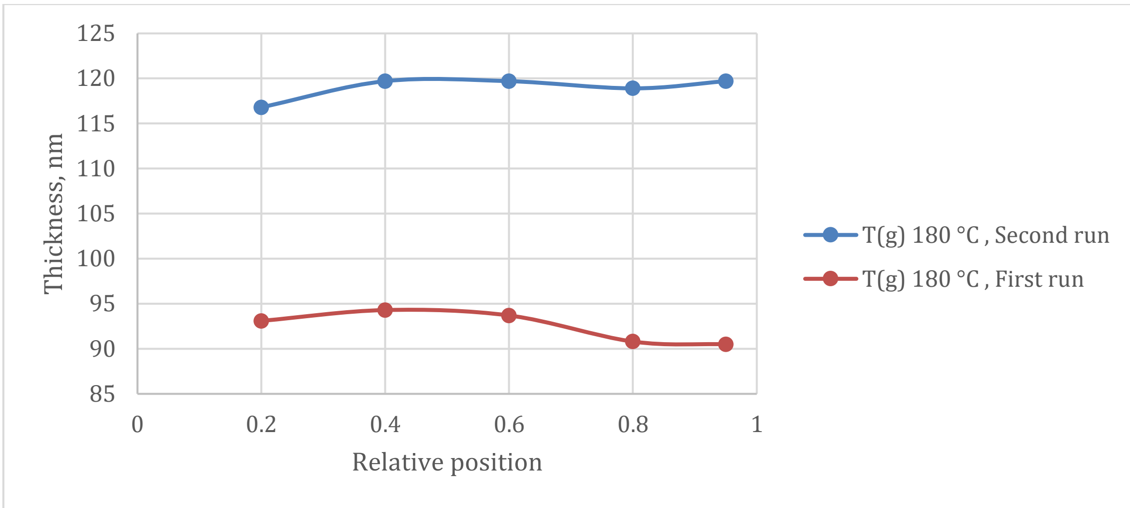

Figure 45: Thickness vs T(g), 1200 cycles, anomalies for 180 C° depositions

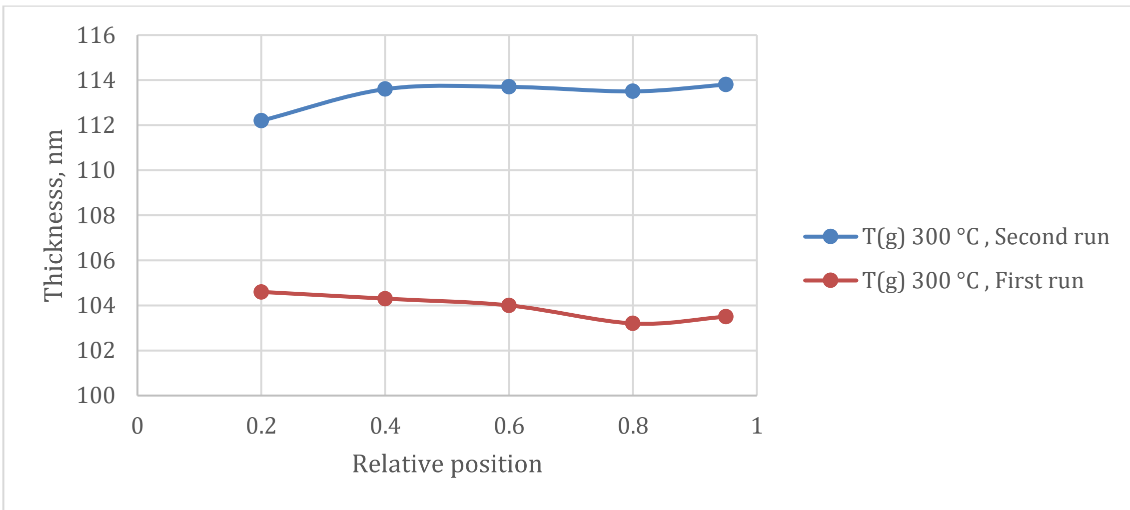

Figure 46: Thickness vs T(g), 1200 cycles, anomalies for 300 C° depositions

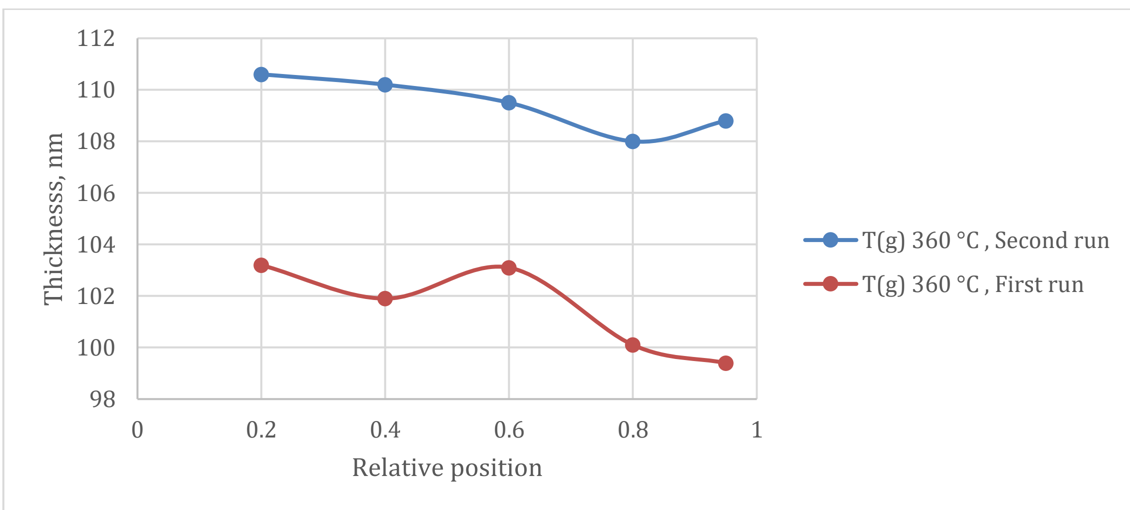

Figure 47: Thickness vs T(g), 1200 cycles, anomalies for 360 C° depositions

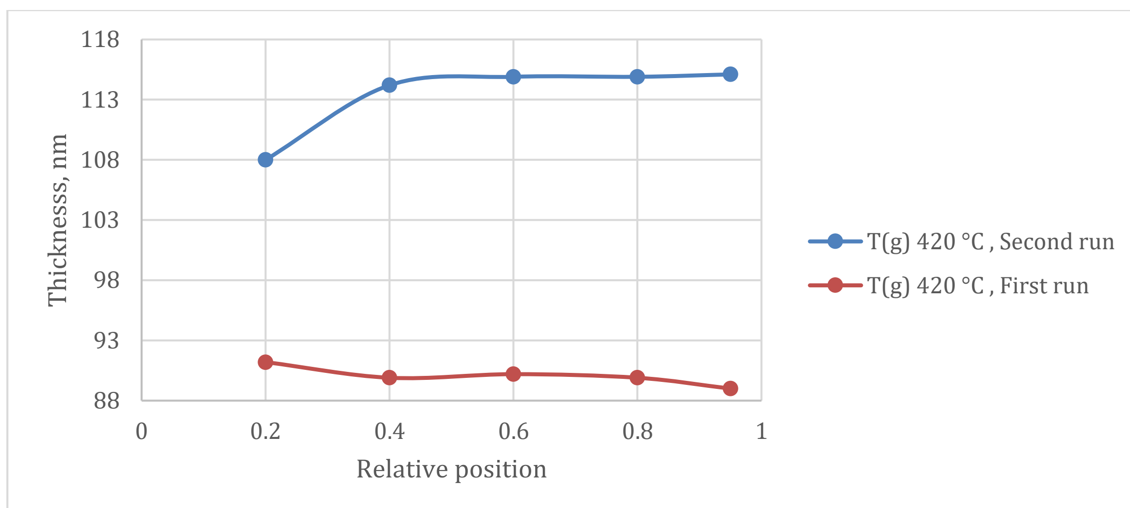

Figure 48: Thickness vs T(g), 1200 cycles, anomalies for 420 C° depositions

Table 7. Thickness vs T(g), 1200 cycles, deviation

	Average thickness result, nm		
Temperature, °C	First run	Second run	Third run
120	102.42	118.28	106.18
180	92.48	118.96	
300	103.92	113.36	
360	101.54	109.42	
424	90.04	113.42	

The first possible explanation for this phenomenon was the frequent evaporation of the AHEAD precursor over multiple days, which could result in a reduction in the reactivity of the AHEAD precursor. This way the "freshness" of precursor dosage can be an important factor while usage of hexakis(ethylamino)disilane in thin depositions.

However, during work with reactor in was noticed by instructor what the reactor may had some issues with integrity. It was assumed that reactor may had leakage issue, which was produced by usage of an old tube in its construction (Figure 49). After replacing the tube, the thickness of resulted films at some point increased which can be noticed on Table 7 (Figure 44 - Figure 48).

Although, the data from deposition with old part of reactor can be considered faulty, it still shows general trends of uniformity and ALD window behaviour, with exception in thickness results and do not alter overall picture.

This way it can be said that these results are still usable and it also a good idea to check your equipment before and during any depositions.

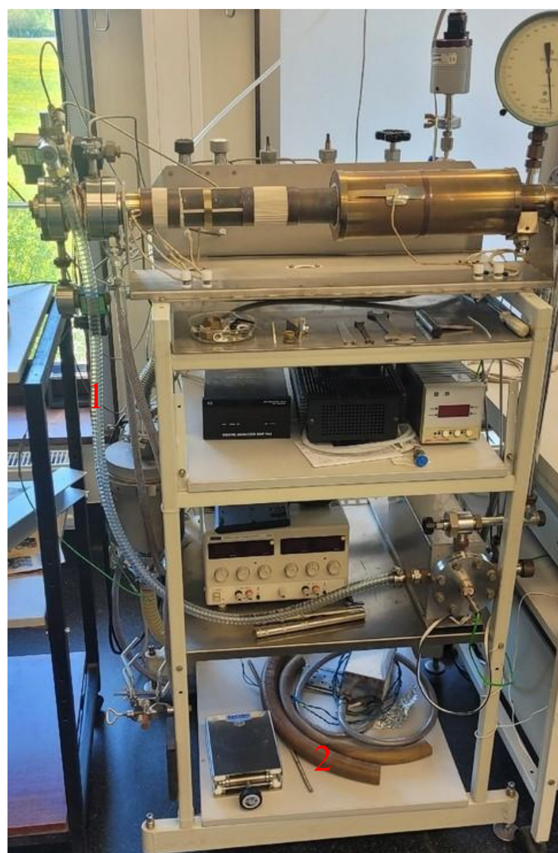

Figure 49. 1 - New tube installed, 2 - Example of previous tube

Non-exclusive licence to reproduce the thesis and make the thesis public

I, Sergei Tolbin ,
(author´s name)

1. grant the University of Tartu a free permit (non-exclusive licence) to

   reproduce, for the purpose of preservation, including for adding to the digital archives of the University of Tartu until the expiry of the term of copyright, my thesis

   Investigation of the Atomic Layer Deposition principles: Effects of growth parameters on SiO_2 thin films using hexakis(ethylamino)disilane (AHEAD) as a silicon precursor ,
   (title of thesis)

   supervised by **Taivo Jõgiaas** ;
   (supervisor´s name)

2. grant the University of Tartu a permit to make the thesis specified in point 1 available to the public via the web environment of the University of Tartu, including via the digital archives, under the Creative Commons licence CC BY NC ND 4.0, which allows, by giving appropriate credit to the author, to reproduce, distribute the work and communicate it to the public, and prohibits the creation of derivative works and any commercial use of the work until the expiry of the term of copyright;

3. am aware of the fact that the author retains the rights specified in points 1 and 2;

4. confirm that granting the non-exclusive licence does not infringe other persons' intellectual property rights or rights arising from the personal data protection legislation.

author's name: Sergei Tolbin

21/07/2025